

DEPENDENCE OF ACOUSTIC SURFACE GRAVITY ON GEOMETRIC CONFIGURATION OF MATTER FOR AXIALLY SYMMETRIC BACKGROUND FLOWS IN THE SCHWARZSCHILD METRIC

PRATIK TARAFDAR

*S. N. Bose National Centre for Basic Sciences, Block JD, Sector III, Salt Lake, Kolkata, India.
pratik.tarafdar@bose.res.in*

TAPAS K. DAS

*Harish Chandra Research Institute, Chhatnag Road, Jhansi, Allahabad 211019, UP, India.
tapas@hri.res.in*

Received Day Month Year

Revised Day Month Year

In black hole evaporation process, the mass of the hole anti-correlates with the Hawking temperature. This indicates that the smaller holes have higher surface gravity. For analogue Hawking effects, however, the acoustic surface gravity is determined by the local values of the dynamical velocity of the stationary background fluid flow and the speed of propagation of the characteristic perturbation embedded in the background fluid, as well as by their space derivatives evaluated along the direction normal to the acoustic horizon, respectively. The mass of the analogue system - whether classical or quantum - does not directly contribute to extremise the value of the associated acoustic surface gravity. For general relativistic axially symmetric background fluid flow in the Schwarzschild metric, we show that the initial boundary conditions describing such accretion influence the maximization scheme of the acoustic surface gravity and associated analogue temperature. Aforementioned background flow onto black holes can assume three distinct geometric configurations. Identical set of initial boundary conditions can lead to entirely different phase-space behavior of the stationary flow solutions, as well as the salient features of the associated relativistic acoustic geometry. This implies that it is imperative to investigate how the measure of the acoustic surface gravity corresponding to the accreting black holes gets influenced by the geometric configuration of the inflow described by various thermodynamic equations of state. Such investigation is useful to study the effect of Einsteinian gravity on the non-conventional classical features as observed in Hawking like effect in a dispersive medium in the limit of a strong dispersion relation.

Keywords: Accretion disc, Black hole physics, Hydrodynamics, Analogue gravity

PACS numbers: 04.40.Dg, 04.70.Dy, 95.30.Sf

1. Introduction

Black hole analogues are fluid dynamical analogue of the black hole space time as perceived in the general theory of relativity.¹⁻⁸ Such analogue systems may be realized by studying the propagation of small amplitude linear perturbation through a dissipationless, irrotational, barotropic transonic fluid. Contemporary research

in the field of analogue gravity phenomena has gained widespread currency since it opens up the possibility of understanding the salient features of the horizon related effects through experimentally realizable physical configurations within the laboratory set up.

Conventional works in this direction, however, concentrate on systems not directly subjected to the gravitational force. Gravity like effects are manifested as emergent phenomena. In such cases, only the Hawking like effects can be studied and no direct connection can be made to such effects with the general relativistic Hawking effects since such non gravitating systems do not include any source of strong gravity capable of producing the Hawking radiation.

To explore whether (and how) the emergent gravity phenomena may be observed in a physical system which itself is under the influence of a strong gravitational field, a series of recent works describe how the acoustic geometry may be realized for stationary, spherically and axially symmetric hydrodynamic flow onto astrophysical black holes.^{9–16}

Accreting black holes represent systems which simultaneously contain gravitational as well as acoustic horizons and are shown to be natural examples of large scale classical analogue systems found in the universe. This allows us to study the influence of the original background black hole space time metric on the embedded perturbative acoustic metric.

Axisymmetric, general relativistic, low angular momentum, inviscid hydrodynamic accretion onto non-rotating astrophysical black holes can be studied for three different geometric configurations of matter – disc accretion with constant flow thickness (hereafter constant height flow), quasi-spherical accretion in conical configuration (hereafter conical flow), and for axisymmetric flow maintained in the hydrostatic equilibrium along the vertical direction (hereafter vertical equilibrium flow). Details about such geometric configurations can further be found in¹⁵ and in section 4 of.¹⁷ For these three geometric configurations, the nature of the sonic geometry embedded within the infalling material has recently been studied for accretion processes under the influence of the generalized post-Newtonian pseudo-Schwarzschild potentials.¹⁷

In our present work, we would like to extend such calculations on a more formal foundation. We shall study the properties of the sonic geometry for general relativistic axisymmetric accretion (resulting in the existence of a curved background geometry for the stationary fluid configuration) onto a Schwarzschild black hole for three different geometric configurations of non self gravitating matter and for each configuration, two different thermodynamic equations of state. We would like to understand how crucial is the role of the relativistic gravitation as well as the geometric configuration of the background stationary flow (subjected to that gravitational field) in determining the essential features of the analogue gravity phenomena. We thus intend to demonstrate how the estimation of the acoustic surface gravity κ gets influenced by the geometric configuration of matter for *general*

relativistic background matter flow onto a Schwarzschild black hole.

For canonical Hawking effect in connection to a Schwarzschild black hole, the Hawking temperature $T_{\text{AH}} \propto \frac{1}{M_{\text{BH}}}$ (M_{BH} being the mass of the Hawking radiating black hole). This indicates that one requires a black hole of reasonably small mass – e.g., a primordial black hole of cosmological origin – to maximize the observable Hawking effect. The extremisation of the observable Hawking effect can thus be parameterized by the mass of the black hole only. One can not have such a straight forward (anti) correlation available for the analogue temperature with the mass parameter of the system to conclude that the acoustic black hole of microscopic dimension will indeed produce a larger analogue temperature. Extremisation of such temperature as well as κ depends on various initial boundary conditions determining the background stationary states of the system under consideration.

2. Acoustic surface gravity (κ) for accreting black hole systems

For a stationary flow configuration, the acoustic horizon is the surface defined by the equation

$$u_{\perp}^2 - c_s^2 = 0, \quad (1)$$

where c_s is position dependent sound speed (the speed of propagation of the perturbation under consideration in general), the bulk flow velocity u_{\perp} is measured along the direction normal to the acoustic horizon.

For any general flow model in Minkowskian spacetime, the acoustic surface gravity κ measured at the acoustic horizon r_h can be obtained as^{1,3}

$$\kappa \propto \left[c_s \frac{\partial}{\partial \eta} (c_s - u_{\perp}) \right]_{r_h}, \quad (2)$$

where space gradient $\partial/\partial\eta$ is taken along the normal to the acoustic horizon. The subscript r_h indicates that the quantities under consideration have been evaluated on acoustic horizon.

Corresponding relativistic generalization of the expression of the acoustic surface gravity is expressed as^{4,11,12}

$$\kappa = \left[\frac{\sqrt{\chi^{\mu}\chi_{\mu}}}{(1 - c_s^2)} \frac{\partial}{\partial \eta} (u_{\perp} - c_s) \right]_{r_h}, \quad (3)$$

where χ^{μ} is the Killing field which is null on the corresponding acoustic horizon. In subsequent sections, we will show that the explicit expression for the norm of χ^{μ} can be evaluated in terms of the values of the background metric elements evaluated on the acoustic horizon and on certain flow parameters.

One needs to calculate the location of the acoustic horizon r_h for a stationary configuration, as well as to evaluate the expression for the normal bulk flow velocity u_{\perp} and the speed of the propagation of the acoustic perturbation c_s along with their space gradients normal to the acoustic horizon to compute the value of κ .

For the background stationary accretion solutions considered in the present work, r_h and $[u, c_s, du/dr, dc_s/dr]$ (evaluated on r_h) is determined using the initial boundary conditions defined by the triad $[\mathcal{E}, \lambda, \gamma]$ for the polytropic accretion and the diad $[T, \lambda]$ for the isothermal accretion, where $\mathcal{E}, \lambda, \gamma$ and T are the specific total conserved energy, specific conserved angular momentum, the adiabatic index ($\gamma = c_p/c_v$, where c_p and c_v are specific heats at constant pressure and volume, respectively), and the bulk ion temperature of the accreting matter, respectively. Extremisation of κ , as will be shown in the subsequent sections, nonlinearly depends on $[\mathcal{E}, \lambda, \gamma]$ and on $[T, \lambda]$ for the adiabatic and the isothermal flows, respectively. One thus needs to explore the three dimensional parameter space spanned by $[\mathcal{E}, \lambda, \gamma]$ and the two dimensional parameter space spanned by $[T, \lambda]$ to apprehend what values of the initial boundary conditions are favoured for the extremisation of κ . This might help to enhance the possibility of obtaining the observable signature of the analogue radiation. One also needs to understand which one out of these three flow configurations favours the production of reasonably large value of κ .

This enables one to provide a ‘calibration space’ spanned by various astrophysically relevant parameters governing the flow, for which the extremisation of κ can be performed. This also provides a comprehensive idea about the influence of the geometric configuration of the black hole accretion flow on the extremisation process of κ .

At this point, it is important to clarify that the present work does not make any attempt to understand the thermal properties of the Hawking like effects. We do not intend to analyze the analogue radiation – its origin, propagation and observational manifestation. We rather concentrate to explore the underlying sonic geometry through the detailed study of the dependence of κ on various factors governing the stationary background configuration. This does not involve the detailed analysis of quantum acoustic Hawking process at least at this stage. We do not deal with the quantization process of the associated phonon field. To accomplish that task, one needs to demonstrate that the effective action for the acoustic perturbation is equivalent to a field theoretic action in curved space, and the associated commutation relation as well as the dispersion relation will directly follow.^{2,8} Such considerations are rather involved and is clearly beyond the scope of our present work. Our main motivation is rather to employ the analogy to describe the classical perturbation of the fluid flow in terms of a field satisfying the wave equation in an effective geometry and to study the consequences relevant to a large-scale gravitating system. We believe that κ itself is a rather important entity to understand the flow structure as well as the associated sonic metric, irrespective of the existence of quantum Hawking like phenomena characterized by their feeble temperature too difficult to detect experimentally.

The significant role of κ in influencing the non negligible classical effects associated with the emergence of the stimulated Hawking effects through the modified dispersion relations at the sonic horizon has recently been emphasized from the the-

oretical front,^{23,24} as well as within the experimental framework in the laboratory set up.^{19–22} The deviation of the Hawking like effects in a dispersive medium from the original Hawking effect is sensitive to the spatial velocity gradient corresponding to the stationary solutions of the background fluid flow.^{23,24} For relativistic accretion onto a Schwarzschild black hole, the expression for κ is found to be an analytical function of the space gradient of the steady state bulk velocity of the background fluid. Such velocity gradient influences the universality of the Hawking like radiation (as well as the departure from it), and various other properties of the anomalous scattering of the acoustic mode due to the modified dispersion relation at the acoustic horizon.

One of the main importances of our work is to identify a natural large-scale gravitating relativistic system where there is a probability to estimate the aforementioned deviation. For such a system the *exact value* of the space gradient of the flow velocity can *explicitly* be computed in terms of realistic, observationally measurable, astrophysically relevant physical entities. It is surely a step ahead of some abstract theoretical calculation as we believe. Existing works which study the anomalous dispersion relation, consider the gradient of the bulk velocity only and the space gradient of the sound speed is not taken into account in any such literature. For adiabatic flow, the speed of propagation of the linear perturbation embedded within the fluid is a position dependent quantity, the role of the gradient of the sonic velocity in influencing the estimation of the deviation of the Hawking like effect from universality cannot be underestimated. In our work we calculate the space gradient of the sonic velocity in terms of the observationally obtainable physical quantities and include such factors in the calculation of κ . Our work can contribute to enrich the formalism as presented in^{23,24} in a more realistic way.

In what follows, we describe our overall scheme for the computation of κ in terms of various flow geometries and for different thermodynamic equations of state.

Hereafter, any relevant distance will be scaled in units of GM_{BH}/c^2 and any velocity will be scaled by the velocity of light in vacuum, c , where M_{BH} represents the mass of the black hole and G represents the universal gravitational constant.

For adiabatic accretion, the equation of state of the form

$$p = K\rho^\gamma \quad (4)$$

is considered to describe the flow. γ is assumed to be constant throughout the flow in the steady state. A more realistic flow model, however, perhaps requires the implementation of a non constant polytropic index having a functional dependence on the radial distance of the form $\gamma \equiv \gamma(r)$.^{41–45} We, nevertheless, have performed our calculations for a reasonably wide spectrum of γ and thus believe that the whole astrophysically relevant range of polytropic indices is covered in our analysis. The proportionality constant K in eq. (4) is a measure of the specific entropy of the accreting fluid provided no additional entropy generation takes place.

Isothermal accretion is assumed to be described by the following equation of

state

$$p = \rho c_s^2 = \frac{\mathcal{R}}{\mu} \rho T = \frac{\rho \kappa_B T}{\mu m_H} \quad (5)$$

$\mathcal{R}, \kappa_B, T, \mu$ and m_H are the universal gas constant, the Boltzmann constant, the isothermal flow temperature, the reduced mass and the mass of the Hydrogen atom, respectively. c_s in the above equation represents the position independent isothermal sound speed which implies that $dc_s/dr = 0$ identically. For isothermal accretion, only the space gradient of the bulk advective velocity, and not that of the speed of propagation of the acoustic perturbation, contributes to the estimation of the acoustic surface gravity.

For energy momentum tensor corresponding to an ideal fluid considered in a Boyer-Lindquist³⁹ line element for a non rotating black hole, we demonstrate (see subsequent sections for detailed derivation) that κ can be expressed as

$$\kappa = \left[\frac{r-2}{r^2(1-c_s^2)} \sqrt{r^2 - \lambda^2 \left(1 - \frac{2}{r}\right)} \left(\frac{du}{dr} - \frac{dc_s}{dr} \right) \right]_{r_h} = f[r, u, c_s, du/dr, dc_s/dr]_{r_h} \quad (6)$$

In subsequent sections, we provide the expressions for $[u, c_s, du/dr, dc_s/dr]_{r_h}$ for three different flow configurations for the adiabatic as well as the isothermal (for which dc_s/dr will vanish everywhere, including at the acoustic horizon, for obvious reason) equation of state. We use those values to study the dependence of κ on various flow parameters as well as on various flow geometries.

3. Overall solution scheme

We consider low angular momentum axially symmetric accretion and the viscous transport of angular momentum has not been taken into account. Such low angular momentum inviscid flow is not a theoretical abstraction. For astrophysical systems, such sub-Keplerian weakly rotating flows are exhibited in various physical situations, such as detached binary systems fed by accretion from OB stellar winds,^{25,27} semi-detached low-mass non-magnetic binaries,²⁸ and super-massive black holes fed by accretion from slowly rotating central stellar clusters (^{29,30} and references therein). Even for a standard Keplerian accretion disc, turbulence may produce such low angular momentum flow (see, e.g.,³¹ and references therein). Reasonably large radial advective velocity for the slowly rotating sub-Keplerian flow implies that the infall time scale is considerably small compared to the viscous time scale for the flow profile considered in this work. Large radial velocities even at larger distances are due to the fact that the angular momentum content of the accreting fluid is relatively low.³²⁻³⁴ The assumption of inviscid flow for the accretion profile under consideration is thus justified from an astrophysical point of view. Such inviscid configuration has also been addressed by other authors using detailed numerical simulation works.^{34,35} The general relativistic Euler and the continuity equations are thus obtained using the vanishing of the four divergence of the energy momentum tensor of an *ideal fluid*.

Considering the flow to be steady and the steady state to be a stable state^a, the time independent Euler and the continuity equations will then be integrated to obtain the respective integrals of motion, since the time independent Euler and the continuity equations are examples of first order ordinary homogeneous differential equations in advective velocity. The integral solution of the Euler equation provides the conserved total specific energy (denoted by \mathcal{E} in this work) as the first integral of motion for polytropic accretion. For isothermal flow, the corresponding first integral of motion (denoted by ξ in this work) cannot be identified with the specific energy of the flow since energy exchange with the surrounding is required to maintain the space invariance of the bulk temperature. The first integral of motion obtained from the Euler equation does not depend on the geometric configuration of the flow.

The equation of continuity implies the conservation of mass and hence its integral solution will provide the mass accretion rate (denoted by \dot{M} in this work) as another first integral of the motion. Explicit expression for the mass accretion rate may not depend on the equation of state used and is found to be a function of the flow thickness. \dot{M} explicitly depends on the flow geometry. For polytropic accretion, we will have three different expressions for \dot{M} for different flow geometries and for the isothermal accretion will have same set of expressions for \dot{M} for flow with constant thickness and conical flow, but the explicit expression will be different for accretion in the vertical equilibrium. This is due to the fact that for accretion in vertical equilibrium the expression for the flow thickness comes out to be a function of the corresponding sound speed. We solve six different cases in this work, three different flow models for a particular energy first integral for the polytropic flow as well as for the first integral corresponding to the isothermal flow.

Once the first integrals of motion are obtained, we find the space gradient of the dynamical velocity u and that of the sonic velocity c_s (for isothermal flow c_s is position independent) and perform the critical point analysis to find out the critical point(s) of the flow. For all flow models other than the flow in vertical equilibrium, the critical points coincide with the sonic points. For flow in vertical equilibrium, critical surfaces are not isomorphic with the sonic surfaces and the integral flow solutions are to be used to find the sonic point (location of the acoustic horizon) by integrating the flow starting from the corresponding saddle type critical points. We study the dependence of κ on $[\mathcal{E}, \lambda, \gamma]$ and on $[T, \lambda]$ for the polytropic as well as for the isothermal accretion, respectively. We compare such dependence for three different flow profiles.

Hereafter, the subscripts CH, CF and VE will indicate that the quantities are evaluated/expressions are formulated for flow with constant height (CH), for quasi spherical conical flow (CF), and for flow in hydrostatic equilibrium along the vertical direction (VE), respectively.

^aOne can perform a linear stability analysis to ensure that the steady axially symmetric inviscid flow is stable, see.⁹⁴

4. Configuration of the background fluid flow

We consider a (3+1) stationary axisymmetric space-time endowed with two commuting Killing fields, within which the dynamics of the background fluid will be studied. For the energy momentum tensor of any ideal fluid with certain equation of state, the combined equation of motion in such a configuration can be expressed as

$$v^\mu \nabla_\mu v^\nu + \frac{c_s^2}{\rho} \nabla_\mu \rho (g^{\mu\nu} + v^\mu v^\nu) = 0, \quad (7)$$

v^μ being the velocity vector field defined on the manifold constructed by the family of streamlines. The normalization condition for such velocity field yields $v^\mu v_\mu = -1$, and c_s is the speed of propagation of the acoustic perturbation embedded inside the bulk flow. ρ is the local rest mass energy density. The local timelike Killing fields $\xi^\mu \equiv (\partial/\partial t)^\mu$ and $\phi^\mu \equiv (\partial/\partial \phi)^\mu$ are the generators of the stationarity (constant specific flow energy is the outcome) and axial symmetry, respectively.

In general, the acoustic ergosphere and the acoustic event horizon do not coincide. However, for a radial flow onto a sink placed at the origin of a stationary axisymmetric geometry they do (see, e.g.,^{4,11} for detail discussion), since only the radial component of the flow velocity $u = u_\perp$ remains non zero everywhere. In this work we consider accretion flow with radial advective velocity u confined on the equatorial plane. The flow will be assumed to have finite radial spatial velocity u (the advective flow velocity as designated in usual astrophysics literature^{37,38}) defined on the equatorial plane of the axisymmetric matter configuration. We focus on stationary solutions of the fluid dynamic equations (to determine the stationary background geometry) and hence consider only the spatial part of such advective velocity. Considering v to be the magnitude of the three velocity, u is the component of three velocity perpendicular to the set of timelike hypersurfaces $\{\Sigma_v\}$ defined by $v^2 = \text{constant}$.

The local radial Mach number M of the accreting fluid is defined as the ratio of the radial component of the local dynamical flow velocity to that of the propagation of the acoustic perturbation embedded inside the accreting matter – $M = u/c_s$. The flow will be locally subsonic or supersonic according to $M < 1$ or > 1 . The flow is transonic if at any moment it crosses the $M = 1$ hypersurface. This happens when a subsonic to supersonic or supersonic to subsonic transition takes place either continuously or discontinuously. Such a point where such crossing takes place continuously is called a sonic point, and where such transition takes place discontinuously is called a shock or a discontinuity. The particular value of the radial distance r for which $M = 1$, is referred as the transonic point or the sonic point, and will be denoted by r_s hereafter. r_s and r_h is thus identical for a transonic system. For $r < r_s$, infalling matter becomes supersonic. Any acoustic perturbation created in such a region is destined to be dragged towards the black hole, and can not escape to the domain $r > r_s$. In other words, any co-moving observer from $r < r_s$ region can not communicate with any observer (co-moving or stationary) located in

the sub-domain $r > r_s$ by sending any signal which travels with velocity $v_{\text{signal}} \leq c_s$, where c_s is defined as the velocity of propagation of the acoustic perturbation (the sound speed) embedded in the moving fluid. Hence the hypersurface through r_s is generated by the acoustic null geodesics, i.e., by the phonon trajectories, and is actually an acoustic horizon for stationary configuration, which is produced when accreting fluid makes a transition from subsonic ($M < 1$) to the supersonic ($M > 1$) state.

At a distance far away from the black hole, accreting material almost always remains subsonic (except possibly for the supersonic stellar wind fed accretion) since it possesses negligible dynamical flow velocity. On the other hand, the flow velocity will approach the velocity of light c while crossing the event horizon, while the maximum possible value of sound speed, even for the steepest possible equation of state, would be $c/\sqrt{3}$,^{37,38} resulting $M > 1$ close to the event horizon. In order to satisfy such inner boundary condition imposed by the event horizon, accretion onto black holes exhibit transonic properties in general.²⁶

For a transonic flow as perceived within the aforementioned configuration, the collection of the sonic points (where the radial Mach number, the ratio of the advective velocity and the speed of propagation of the acoustic perturbation in the radial direction, becomes unity) at a specified radial distance forms the acoustic horizon, the generators of which are the phonon trajectories. An axially symmetric transonic black hole accretion can thus be considered as a natural example of the classical analogue gravity model which contains two different horizons, the gravitational (corresponding to the accreting black hole) as well as the acoustic (corresponding to the transonic fluid flow).

To describe the flow structure in further detail, the energy momentum tensor of an ideal fluid of the form

$$T^{\mu\nu} = (\epsilon + p)v^\mu v^\nu + pg^{\mu\nu} \quad (8)$$

is considered in a Boyer-Lindquist³⁹ line element normalized for $G = c = M_{\text{BH}} = 1$ and $\theta = \pi/2$ as defined below⁴⁰

$$ds^2 = g_{\mu\nu}dx^\mu dx^\nu = -\frac{r^2\Delta}{A}dt^2 + \frac{A}{r^2}(d\phi - \omega dt)^2 + \frac{r^2}{\Delta}dr^2 + dz^2, \quad (9)$$

where

$$\Delta = r^2 - 2r + a^2, A = r^4 + r^2a^2 + 2ra^2, \omega = 2ar/A, \quad (10)$$

a being the Kerr parameter related to the black holes spin angular momentum. The required metric elements are:

$$g_{rr} = \frac{r^2}{\Delta}, g_{tt} = \left(\frac{A\omega^2}{r^2} - \frac{r^2\Delta}{A}\right), g_{\phi\phi} = \frac{A}{r^2}, g_{t\phi} = g_{\phi t} = -\frac{A\omega}{r^2}. \quad (11)$$

The specific angular momentum λ (angular momentum per unit mass) and the

angular velocity Ω can thus be expressed as

$$\lambda = -\frac{v_\phi}{v_t}, \quad \Omega = \frac{v^\phi}{v^t} = -\frac{g_{t\phi} + \lambda g_{tt}}{g_{\phi\phi} + \lambda g_{t\phi}}. \quad (12)$$

We also define

$$B = g_{\phi\phi} + 2\lambda g_{t\phi} + \lambda^2 g_{tt}, \quad (13)$$

which will be used in the subsequent sections to calculate the value of the acoustic surface gravity.

For flow onto a Schwarzschild black hole, one can obtain the respective metric elements (and hence, the expression for λ and B thereof) by substituting $a = 0$ in eq. (10 - 13). We construct a Killing vector $\chi^\mu = \xi^\mu + \Omega\phi^\mu$ where the Killing vectors ξ^μ and ϕ^μ are the two generators of the temporal and axial isometry groups, respectively. Once Ω is computed at the acoustic horizon r_h , χ^μ becomes null on the transonic surface. The norm of the Killing vector χ_μ may be computed as

$$\sqrt{|\chi^\mu \chi_\mu|} = \sqrt{(g_{tt} + 2\Omega g_{t\phi} + \Omega^2 g_{\phi\phi})} = \frac{\sqrt{\Delta B}}{g_{\phi\phi} + \lambda g_{t\phi}}. \quad (14)$$

Hence the explicit form of the acoustic surface gravity for relativistic flow onto a Schwarzschild black hole looks like

$$\kappa = \left[\frac{\sqrt{r^2 - 2r}}{r^2 (1 - c_s^2)} \sqrt{\frac{g_{\phi\phi} + \lambda^2 g_{tt}}{g_{rr}}} \left(\frac{du}{dr} - \frac{dc_s}{dr} \right) \right]_{r_h} \quad (15)$$

5. The first integrals of motion

Vanishing of the four divergence of the energy momentum tensor provides the general relativistic version of the Euler equation

$$T^{\mu\nu}_{;\nu} = 0. \quad (16)$$

whereas the corresponding continuity equation is obtained from

$$(\rho v^\mu)_{;\mu} = 0. \quad (17)$$

The time independent part of the linear momentum conservation equation (Euler equation) is a first order homogeneous differential equation. Its integral solution will provide a constant of motion (first integral of motion) for whatever equation of state is used to describe the accreting matter. Such first integral of motion, however, cannot formally be identified with the total energy of the background fluid flow for any equation of state other than the polytropic one.

5.1. Integral solution of the linear momentum conservation equation

5.1.1. Polytropic accretion

For polytropic accretion, the specific enthalpy h is formulated as

$$h = \frac{p + \epsilon}{\rho}, \quad (18)$$

where the energy density ϵ includes the rest mass density and internal energy and is defined as

$$\epsilon = \rho + \frac{p}{\gamma - 1} \quad (19)$$

The adiabatic sound speed c_s is defined as

$$c_s^2 = \left(\frac{\partial p}{\partial \epsilon} \right)_{\text{constant enthalpy}} \quad (20)$$

At constant entropy, the enthalpy can be expressed as

$$h = \frac{\partial \epsilon}{\partial \rho} \quad (21)$$

and hence

$$h = \frac{\gamma - 1}{\gamma - (1 + c_s^2)} \quad (22)$$

Contracting eq. (16) with ϕ^μ one obtains (since $\phi^\nu p_{,\nu} = 0$, $\phi^\mu = \delta^\mu_\phi$, and $g_{\mu\lambda;\nu} = 0$)

$$[\phi_\mu h v^\mu]_{,\nu} = 0. \quad (23)$$

Since $\phi_\mu h v^\mu = h v_\phi$, the angular momentum per baryon for the axisymmetry flow is conserved. Contraction of eq. (16) with ξ^μ provides

$$\xi^\mu [\xi_\mu T^{\mu\nu}]_{,\nu} = 0 \quad (24)$$

from where the quantity $h v_t$ comes out as one of the first integrals of motion of the system. $h v_t$ is actually the relativistic version of the Bernoulli's constant⁴⁷ and can be identified with the total specific energy of the general relativistic ideal fluid \mathcal{E} (see, e.g.,⁴⁸ and references therein) scaled in units of the rest mass energy. Hence $\mathcal{E} = h v_t$

From the normalization condition $v^\mu v_\mu = -1$ one obtains

$$v_t = \sqrt{\frac{g_{t\phi}^2 - g_{tt}g_{\phi\phi}}{(1 - \lambda\Omega)(1 - u^2)(g_{\phi\phi} + \lambda g_{t\phi})}} \quad (25)$$

We thus obtain

$$\mathcal{E} = \frac{\gamma - 1}{\gamma - (1 + c_s^2)} \sqrt{\frac{g_{t\phi}^2 - g_{tt}g_{\phi\phi}}{(1 - \lambda\Omega)(1 - u^2)(g_{\phi\phi} + \lambda g_{t\phi})}} \quad (26)$$

The exact form for \mathcal{E} will depend on the space time structure appearing in the expression for \mathcal{E} through the metric elements. It will not depend on the matter geometry since the accretion is assumed to be non self gravitating. For isothermal flow, the total specific flow energy does not remain constant, rather the first integral of motion obtained by integrating the relativistic Euler equation has a different algebraic form which can not be identified with the total energy of the system.

5.1.2. Isothermal flow

For isothermal flow, the system has to dissipate energy to keep the temperature constant. The isotropic pressure is proportional to the energy density through

$$p = c_s^2 \epsilon \quad (27)$$

From the time part of eq. (16), one obtains

$$\frac{dv_t}{v_t} = -\frac{dp}{p + \epsilon} \quad (28)$$

Using the definition of enthalpy, the above equation may be re-written as

$$\frac{dv_t}{v_t} = -\frac{1}{h} \frac{dp}{d\rho} \frac{d\rho}{\rho} \quad (29)$$

Since the isothermal sound speed can be defined as (see, e.g.,⁴⁹ and references therein)

$$c_s = \sqrt{\frac{1}{h} \frac{dp}{d\rho}} \quad (30)$$

we obtain

$$\ln v_t = -c_s^2 \ln \rho + A, \text{ where } A \text{ is a constant} \quad (31)$$

Which further implies that

$$v_t \rho^{c_s^2} = \xi \quad (32)$$

Hence ξ is the first integral of motion for the isothermal flow, which is not to be confused with the total conserved specific energy \mathcal{E} .

Owing to the Clayperon-Mendeleev equation^{67,68}

$$c_s = \sqrt{\frac{k_B}{\mu m_H} T} \quad (33)$$

space invariance of temperature requires the sound speed to be position independent for isothermal accretion, and hence the space gradient of the speed of propagation of the isothermal perturbation does not contribute to the estimation of the acoustic surface gravity. The expression for the first integral of motion obtained

from the integral solution of the Euler equation is independent of the geometrical configuration of matter as already discussed, and is found to be

$$\xi = \frac{r^2(r-2)}{(r^3 - (r-2)\lambda^2)(1-u^2)} \rho^{2c_s^2} \quad (34)$$

5.2. Integral solution of the mass conservation equation

For $g \equiv \det(g_{\mu\nu})$, the mass conservation equation (17) implies

$$\frac{1}{\sqrt{-g}} (\sqrt{-g} \rho v^\mu)_{,\mu} = 0, \quad (35)$$

which further leads to

$$[(\sqrt{-g} \rho v^\mu)_{,\mu} d^4x = 0] \quad (36)$$

$\sqrt{-g} d^4x$ being the co-variant volume element. We assume that there is no convection current along any non equatorial direction, and hence no non-zero terms involving v^θ (for spherical polar co-ordinate) or v^z (for flow studied within the framework of cylindrical co-ordinate) should become significant. This assumption leads to the condition

$$\partial_r (\sqrt{-g} \rho v^r) dr d\theta d\phi = 0, \quad (37)$$

for the stationary background flow studied using the spherical polar co-ordinate (r, θ, ϕ) and

$$\partial_r (\sqrt{-g} \rho v^r) dr dz d\phi = 0, \quad (38)$$

for such flow studied using the cylindrical co-ordinate (r, ϕ, z) .

We integrate eq. (37) for $\phi = 0 \rightarrow 2\pi$ and $\theta = -H_\theta \rightarrow H_\theta$; $\pm H_\theta$ being the value of the polar co-ordinates above and below the equatorial plane, respectively, for a local flow half thickness H , to obtain the conserved mass accretion rate \dot{M} in the equatorial plane. The integral solution of the mass conservation equation – the mass accretion rate \dot{M} – comes out to be another first integral of motion for our stationary background fluid configuration. For conical wedge shaped flow studied in the spherical polar co ordinate, $2H/r$ remains constant. Flow with such geometric configuration was first studied by⁵⁰ and followed by⁵¹ for pseudo-Schwarzschild flow geometry under the influence of the Paczyński & Wiita⁵² pseudo-Schwarzschild Newtonian like black hole potential. The relativistic version for such flow has further been studied by.^{49,53–61}

In a similar fashion, eq. (38) can be integrated for $z = -H_z \rightarrow H_z$ (where $\pm H_z$ is the local half thickness of the flow) symmetrically over and below the equatorial plane for axisymmetric accretion studied using the cylindrical polar co-ordinate to obtain the corresponding mass accretion rate on the equatorial plane. Contrary to the first integral of motion obtained by integrating the Euler equation for a particular thermodynamic equation of state, the expression for the mass accretion

rate does not explicitly depend on the equation of state, but is different for different geometric configuration of the matter distribution. The general expression for the mass accretion rate can be provided as

$$\dot{M} = \rho v^r \mathcal{A}(r) \quad (39)$$

$\mathcal{A}(r)$ being the two dimensional surface area having surface topology $\mathbb{R}^1 \times \mathbb{R}^1$ or $\mathbb{S}^1 \times \mathbb{S}^1$ through which the inward mass flux is estimated in the steady state. For $\mathbb{S}^1 \times \mathbb{S}^1$ (and for not so large value of θ), $\mathcal{A}(r) = 4\pi H_\theta r^2$, and for $\mathbb{R}^1 \times \mathbb{R}^1$ (axisymmetric accretion studied using the cylindrical co ordinate), $\mathcal{A}(r) = 4\pi H_z r$.

In subsequent sections, we provide the explicit expressions for the conserved mass accretion rate and related quantities for three different flow geometries

6. Stationary transonic accretion solutions

6.1. *polytropic accretion*

We substitute the values of the corresponding metric elements and of Ω in eq. (26) and obtain

$$\mathcal{E} = -\frac{\gamma - 1}{(\gamma - (1 + c_s^2))} \sqrt{\frac{(1 - \frac{2}{r})}{(1 - \frac{\lambda^2}{r^2}(1 - \frac{2}{r}))(1 - u^2)}} \quad (40)$$

In what follows, we shall illustrate the procedure to obtain the stationary transonic flow solutions for flow with constant thickness. We shall then provide the corresponding similar expressions for other flow geometries.

6.1.1. *Flow with constant thickness*

As stated in the paragraphs preceding eq. (39), we integrate the continuity equation to obtain the conserved mass accretion rate to be

$$\dot{M}_{\text{CH}} = 2\pi\rho \frac{u \sqrt{1 - \frac{2}{r}}}{\sqrt{1 - u^2}} rH \quad (41)$$

H being the constant disc height.

Equations (40 – 41) can not directly be solved simultaneously since it contains three unknown variables u, c_s and ρ , all of which are functions of the radial distance r . Any accretion variable from the triad $[u, c_s, \rho]$ has to be eliminated in terms of the other two. We are, however, interested to study the radial Mach number profile to identify the location of the acoustic horizon (the radial distance at which M becomes unity), and hence the study of the radial variation of u and c_s are of prime interest in this case. We would thus like to express ρ in terms of c_s and other related constant quantities. To accomplish the aforementioned task, we make a transformation $\tilde{\Xi} = \dot{M} K^{\frac{1}{\gamma-1}} \gamma^{\frac{1}{\gamma-1}}$. Employing the definition of the sound speed

$c_s^2 = \left(\frac{\partial p}{\partial \epsilon}\right)_{\text{Constant Entropy}}$ as well as the equation of state used to describe the flow, the expression for $\dot{\Xi}$ can further be elaborated as

$$\dot{\Xi}_{\text{CH}} = 2\pi \frac{u \sqrt{1 - \frac{2}{r}}}{\sqrt{1 - u^2}} r c_s^{\frac{2}{\gamma-1}} \left(\frac{\gamma - 1}{\gamma - (1 + c_s^2)} \right)^{\frac{1}{\gamma-1}} H \quad (42)$$

The entropy per particle σ is related to K and γ as⁶⁵

$$\sigma = \frac{1}{\gamma - 1} \log K + \frac{\gamma}{\gamma - 1} + \text{constant}$$

where the constant depends on the chemical composition of the accreting material. The above equation implies that K is a measure of the specific entropy of the accreting matter. We thus interpret $\dot{\Xi}$ as the measure of the total inward entropy flux associated with the accreting material and label $\dot{\Xi}$ to be the stationary entropy accretion rate. The concept of the entropy accretion rate was first introduced in^{50,51} to obtain the stationary transonic solutions of the low angular momentum non relativistic axisymmetric accretion under the influence of the Paczyński and Wiita⁵² pseudo-Schwarzschild potential onto a non rotating black hole.

The conservation equations for \mathcal{E} , \dot{M} and $\dot{\Xi}$ may simultaneously be solved to obtain the complete accretion profile on the radial Mach number vs radial distance phase space, see, e.g.,^{12,48} for the depiction of several such phase portraits.

The relationship between the space gradient of the acoustic velocity and that of the advective velocity can now be established by differentiating eq. (42)

$$\left[\frac{dc_s}{dr} \right]_{\text{CH}} = -\frac{\gamma - 1}{2} \frac{\left\{ \frac{1}{u} + \frac{u}{1 - u^2} \right\} \frac{du}{dr} + \left\{ \frac{1}{r} + \frac{1}{r^2(1 - \frac{2}{r})} \right\}}{\frac{1}{c_s} + \frac{c_s}{\gamma - (1 + c_s^2)}} \quad (43)$$

Differentiation of eq. (40) with respect to the radial distance r provides another relation between dc_s/dr and du/dr . We substitute dc_s/dr as obtained from eq. (43) into that relation and finally obtain the expression for the space gradient of the advective velocity as

$$\left[\frac{du}{dr} \right]_{\text{CH}} = \frac{c_s^2 \left\{ \frac{1}{r} + \frac{1}{r^2(1 - \frac{2}{r})} \right\} - f_2(r, \lambda)}{(1 - c_s^2) \frac{u}{1 - u^2} - \frac{c_s^2}{u}} = \frac{N_1}{D_1} \quad (44)$$

16 *Tarafdar & Das*

where

$$f_2(r, \lambda) = -\frac{\lambda^2}{r^3} \left\{ \frac{1 - \frac{3}{r}}{1 - \frac{\lambda^2}{r^2}(1 - \frac{2}{r})} \right\} + \frac{1}{r^2(1 - \frac{2}{r})} \quad (45a)$$

We define another quantity $f_1(r, \lambda)$ which shall be used later,

$$f_1(r, \lambda) = \frac{3}{r} + \frac{\lambda^2}{r^3} \left\{ \frac{1 - \frac{3}{r}}{1 - \frac{\lambda^2}{r^2}(1 - \frac{2}{r})} \right\} \quad (45b)$$

Eq. (43 – 44) can now be identified with a set of non-linear first order differential equations representing autonomous dynamical systems,⁶⁶ and their integral solutions provide phase trajectories on the radial Mach number M vs the radial distance r plane. The ‘regular’ critical point conditions for these integral solutions are obtained by simultaneously making the numerator and the denominator of eq. (44) vanish. The aforementioned critical point conditions may thus be expressed as

$$[u = c_s]_{r_c}, \quad [c_s]_{r_c} = \sqrt{\frac{f_2(r_c, \lambda)}{\frac{2}{r_c} + \frac{1}{r_c^2(1 - \frac{2}{r_c})}}} \quad (46)$$

Since in this work we deal with a transonic fluid in real space for which the flow is continuous along the entire real line, only the ‘regular’ or ‘smooth’ critical point is considered, for which u, c_s as well as their space derivatives remain regular and do not diverge. Such a critical point may be of saddle type allowing a transonic solution to pass through it, or may be of centre type through which no physical transonic solution can be constructed. Other categories of critical point include a ‘singular’ one for which u, c_s are continuous but their derivatives diverge. All such classifications have been discussed in detail and the criteria for a critical point to qualify as a ‘regular’ one which is associated with a physical acoustic horizon has been found out in.¹¹

Equation (46) provides the critical point condition but not the location of the critical point(s). It is necessary to solve eq. (40) under the critical point condition for a set of initial boundary conditions as defined by $[\mathcal{E}, \lambda, \gamma]$. The value of c_s and u , as obtained from eq. (46), may be substituted in eq. (40) to obtain the following 11th degree algebraic polynomial equation for $r = r_c$, r_c being the location of the critical point

$$a_0 + a_1 r_c + a_2 r_c^2 + a_3 r_c^3 + a_4 r_c^4 + a_5 r_c^5 + a_6 r_c^6 + a_7 r_c^7 + a_8 r_c^8 + a_9 r_c^9 + a_{10} r_c^{10} + a_{11} r_c^{11} = 0 \quad (47)$$

where, the coefficients a_i are functions of $[\mathcal{E}, \lambda, \gamma]$. The explicit form of such coefficients are derived, and the results are presented in the appendices.

A particular set of values of $[\mathcal{E}, \lambda, \gamma]$ will then provide the numerical solution for the algebraic expression to obtain the exact value of r_c . Astrophysically relevant

domain for such initial boundary conditions are⁴⁸ defined by

$$[1 \lesssim \mathcal{E} \lesssim 2, 0 < \lambda \leq 4, 4/3 \leq \gamma \leq 5/3] \quad (48)$$

For accretion with constant height, the critical point condition reveals that the advective velocity and the sound velocity are same at the critical point. Hence the critical surface at r_c and the acoustic horizon r_h coincide for this flow geometry.

For an astrophysically relevant set of $[\mathcal{E}, \lambda, \gamma]$ the critical point(s) of the phase trajectory can be identified, and a linearisation study in the neighbourhood of these critical points(s) may be performed⁶⁶ to develop a classification scheme to identify the nature of the critical point(s). Since viscous transport of angular momentum has not been taken into account in the present work, such critical points are either of saddle type through which a stationary transonic flow solution can be constructed, or of a centre type which does not allow any transonic solution on phase portrait to pass through it. A complete understanding of the background stationary transonic flow topologies on the phase portrait will require a numerical integration of the non analytically solvable non linearly coupled differential equations describing the space gradient of the advective velocity as well as that of the speed of propagation of the acoustic perturbation embedded within the stationary axisymmetric background spacetime.

For a particular set of $[\mathcal{E}, \lambda, \gamma]$, solution of eq. (47) provides either no real positive root lying outside the gravitational black hole horizon implying that no acoustic horizon forms outside the black hole event horizon (non availability of the transonic solution) for that value of $[\mathcal{E}, \lambda, \gamma]$, or provides one, two or three (at most) real positive roots lying outside the black hole event horizon. Typically, if only one root is found, the critical point is of saddle type and a mono-transonic flow profile is obtained with a single acoustic horizon for obvious reason. Solutions containing two critical saddle points imply the presence of a homoclinic orbit^b on the phase plot and hence such solutions are excluded.

Stationary configuration with three critical points requires a somewhat detailed understanding. Although a full description is available in,⁴⁸ we provide a brief account over here for the sake of completeness. One out of the aforementioned three critical points is of centre type which is circumscribed by two saddle type critical points, see, e.g.,⁶⁹ for details about the characteristic features of the saddle and the center type critical points. With reference to the gravitational horizon, one of these saddle points forms sufficiently close to it, even closer than the innermost circular stable orbit. i.e., ISCO (see, e.g.,³⁷ and³⁸ for details about ISCO) in general, and is termed as the inner type critical point. The other saddle type point, termed as the outer saddle type critical point, is usually formed at a fairly large

^bA homoclinic orbit or a homoclinic connection is a bi-asymptotic trajectory converging to a saddle like orbit as time goes to positive or negative infinity. For our stationary systems, a homoclinic orbit on a phase portrait is realized as an integral solution that re-connects a saddle type critical point to itself and embarrasses the corresponding centre type critical point. For a detailed description of such phase trajectories from a dynamical systems point of view, see, e.g.,⁶⁹⁻⁷¹

distance away from the gravitational horizon. The inner critical point thus forms in a region of substantially strong gravitational field whereas the outer type critical point, in many cases, is formed in a region of asymptotically flat spacetime. This is because, depending on the choice of $[\mathcal{E}, \lambda, \gamma]$, such a critical point can be located at a distance $10^6 GM_{BH}/c^2$ (or even more) away from the gravitational horizon. The centre type critical point, termed as the middle critical point because of the fact that $r_c^{inner} < r_c^{middle} < r_c^{outer}$, forms usually at a length scale ranging from 10 to 10^{3-4} in units of GM_{BH}/c^2 , depending on the value of $[\mathcal{E}, \lambda, \gamma]$ used. $[\mathcal{E}, \lambda, \gamma]_{mc} \subset [\mathcal{E}, \lambda, \gamma]$ thus provides the multi-critical behaviour of stationary transonic solution. The parameter space spanned by $[\mathcal{E}, \lambda, \gamma]_{mc}$ can further be classified into two different subspaces for which the representative phase portraits are topologically different. Such subspaces are characterized by the relative values of the stationary entropy accretion rate $\dot{\Sigma}$ evaluated at the inner and the outer critical points, respectively. For $\dot{\Sigma}_{r_c^{inner}} > \dot{\Sigma}_{r_c^{outer}}$, accretion can have three allowed critical points, and a homoclinic orbit is generated through the inner saddle type critical point, whereas for $\dot{\Sigma}_{r_c^{inner}} < \dot{\Sigma}_{r_c^{outer}}$ transonic accretion can have only one saddle type (inner) critical point and the homoclinic orbit forms through the outer saddle type critical point. Hence *only* $[\mathcal{E}, \lambda, \gamma]_{mc}^{\dot{\Sigma}_{r_c^{inner}} > \dot{\Sigma}_{r_c^{outer}}} \subset [\mathcal{E}, \lambda, \gamma]_{mc}$ provides the multi-critical accretion configuration for which two saddle type and one center type (delimited between two such saddle types) critical points are available. As already mentioned, a physically acceptable transonic solution for inviscid accretion cannot be constructed through a centre type critical point. A multi-critical flow with three critical points is thus a theoretical abstraction.

On the other hand, a bi-transonic accretion is a practically realizable configuration where the stationary transonic accretion solution passes through one inner and one outer saddle type sonic points. For flow geometries providing the isomorphism between the critical and the sonic points, such sonic points define the acoustic horizons. For flow configuration which does not allow such isomorphism, a sonic point can be identified on the integral stationary flow solutions corresponding to every saddle type critical point. For a bi-transonic solution, however, it should indeed be realized that a smooth stationary solution can not encounter more than one regular sonic point since once it crosses the outer type sonic point (for accretion) it becomes supersonic and only a subsonic solution can have access to pass through the inner sonic point. No continuous transonic solution can accommodate more than one acoustic horizons. Multi transonicity could only be realized as a specific flow configuration where the combination of two different otherwise smooth solutions passing through two different saddle type critical (and hence sonic) points are connected to each other through a discontinuous shock transition. Such a shock has to be stationary and will be located between two sonic points. For certain $[\mathcal{E}, \lambda, \gamma]_{nss} \subset [\mathcal{E}, \lambda, \gamma]_{mc}^{\dot{\Sigma}_{r_c^{inner}} > \dot{\Sigma}_{r_c^{outer}}}$ where 'nss' stands for no shock solution, three critical points (two saddle embracing a centre one) are routinely obtained but no stationary shock forms for the stationary transonic accretion. Hence

no multi transonicity is observed even if the flow is multi-critical, and real physical accretion solution can have access to only one saddle type critical point (the outer one) out of the two. Thus multi critical accretion and multi transonic accretion are not topologically isomorphic in general. A true multi-transonic flow can only be realized for $[\mathcal{E}, \lambda, \gamma]_{ss} \subset [\mathcal{E}, \lambda, \gamma]_{mc}^{\dot{\epsilon}_c^{inner} > \dot{\epsilon}_c^{outer}}$ where ‘ss’ stands for ‘shock solution’, if the criteria for the energy preserving relativistic Rankine-Hugoniot shock^{72–76} for the adiabatic accretion and temperature preserving relativistic shock^{49,77} for the isothermal accretion are met. In this work, however, we will not be interested to deal with the shock solutions and would mainly concentrate on the mono-transonic flow to study the accretion model dependence of the acoustic surface gravity κ . Further details will be provided in subsequent paragraphs where we describe the methodology of constructing the Mach number vs radial distance (measured from the gravitational horizon in units of GM_{BH}/c^2) phase portrait, see, e.g., figure 2 of⁴⁸ and related discussions may be found therein for details of such multi-transonic shocked accretion flow configurations.

Space gradient of the advective velocity at the critical points for various flow configurations can be obtained by evaluating the limiting values of (du/dr) at such points using the l’Hôpital’s rule.⁸⁶ The expressions for the critical values of (du/dr) and (dc_s/dr) have been provided in the appendix.

The critical acoustic velocity gradient $(dc_s/dr)_{r=r_c}$ can also be computed by substituting the value of $\left(\frac{du}{dr}\right)_{r=r_c}$ in eq. (43) and by evaluating other quantities in eq. (43) at r_c . Both $(dc_s/dr)_{r=r_c}$ and $\left(\frac{du}{dr}\right)_{r=r_c}$ can be reduced to an algebraic expression in r_c with real coefficients that are complicated functions of $[\mathcal{E}, \lambda, \gamma]$. Once r_c is known for a set of values of $[\mathcal{E}, \lambda, \gamma]$, the critical slope for the advective velocity, i.e., the space gradient for u at r_c can be computed as a pure number, which may either be a real number providing a saddle type point (for stationary transonic accretion solution to exist) or an imaginary number for providing a centre type point (no transonic solution can be found).

To obtain the Mach number vs radial distance phase plot for the stationary transonic accretion flow, one needs to simultaneously integrate the set of coupled differential equations (43 – 44) for a specific set of initial boundary conditions determined by $[\mathcal{E}, \lambda, \gamma]$. The initial value of the space gradient of the advective velocity, i.e., the critical velocity gradient evaluated at the critical point and provided in eq. (89) and the critical space gradient of the sound speed can be numerically iterated using the fourth order Runge - Kutta method⁷⁸ to obtain the integral solutions for the mono-transonic as well as for the multi-transonic flow. Details of such numerical integration scheme, along with the representative phase plots are available in.^{12,16,48} Acoustic surface gravity is not relevant for a centre type critical point since no stationary transonic solution can be constructed through such points. For flow with constant thickness and for conical flow – both for the adiabatic as well as the isothermal accretion – saddle type critical points and the sonic points are

isomorphic. Since the critical surface and the acoustic horizon is identical, numerical construction of the integral stationary solution is not required to calculate the corresponding acoustic surface gravity for these flow geometries, and value of $[u, c_s, du/dr, dc_s/dr]_{r_c}$ is all we need to calculate the value of κ for the respective flow configuration. In such cases, for axisymmetric flow with constant height for example, the surface gravity can be computed as

$$\kappa_{\text{Adiabatic}}^{\text{Constant Height}} = \left| \frac{r-2}{r^2(1-c_s^2)} \sqrt{r^2 - \lambda^2 \left(1 - \frac{2}{r}\right)} \left[\eta_1 \frac{du}{dr} + \sigma_1 \right] \right|_{r_c} \quad (49)$$

where

$$\eta_1 = 1 + \frac{\gamma - (1+u^2)}{2(1-u^2)}, \quad \sigma_1 = \left(\frac{\gamma-1}{2} \right) \left(\frac{\frac{1}{r} + \frac{1}{r^2(1-\frac{2}{r})}}{\frac{1}{u} + \frac{u}{\gamma-(1+u^2)}} \right) \quad (50)$$

For accretion in hydrostatic equilibrium along the vertical direction, critical points and the sonic points are not isomorphic. As a result, the acoustic horizon does not form on the critical surface. The location of the sonic point will always be located at a radial distance $r_{\text{sonic}} < r_{\text{critical}}$ (hereafter we will designate a sonic point as r_s instead of r_{sonic}). Such r_s is to be found out by integrating the expression of (du/dr) and (dc_s/dr) and by locating the radial co ordinate on the equatorial plane for which the Mach number becomes exactly equal to unity. Since the condition $u^2 - c_s^2 = 0$ is satisfied at r_s and not at r_c , $[u, c_s, du/dr, dc_s/dr]_{r_s}$ is to be used to calculate the corresponding value of the acoustic surface gravity instead of $[u, c_s, du/dr, dc_s/dr]_{r_c}$ for those particular flow geometries.

It is relevant to note that the absolute value of the (constant) disc thickness H does not enter anywhere in the expression of the acoustic surface gravity (and hence, into the calculation of the Hawking like temperature). Similar result is to be obtained for the conical flow where the geometrical factor (the solid angle) representing the angular opening of the conical flow does not show up in the expression for κ or T_{AH} as well. This implies that it is only the geometrical configuration of the matter (non self gravitating) and not the absolute measure of the flow thickness (for constant height flow) or the ratio of the local height to the local radial distance (for conical flow) which influences the computation of the acoustic surface gravity. This may not be the situation where the radius dependent flow thickness itself is found to be a function of the speed of propagation of acoustic perturbation.

6.1.2. Conical flow model

The mass accretion rate is calculated as

$$\dot{M}_{CF} = \Lambda \rho \frac{u \sqrt{1 - \frac{2}{r}}}{\sqrt{1 - u^2}} r^2 \quad (51)$$

Λ is the geometric factor determining the exact shape of the flow, over which integration of the continuity equation is performed.

The corresponding entropy accretion rate is

$$\left[\dot{\Sigma}\right]_{\text{CF}} = \Lambda \frac{u \sqrt{1 - \frac{2}{r}}}{\sqrt{1 - u^2}} r^2 c_s^{\frac{2}{\gamma-1}} \left(\frac{\gamma-1}{\gamma-(1+c_s^2)}\right)^{\frac{1}{\gamma-1}} \quad (52)$$

The relationship between the corresponding space gradient of the speed of propagation of the acoustic perturbation (the space gradient of the adiabatic sound speed) and that of the stationary advective velocity can be found as

$$\left[\frac{dc_s}{dr}\right]_{\text{CF}} = -\frac{\gamma-1}{2} \frac{\left(\frac{1}{u} + \frac{u}{1-u^2}\right) \left[\frac{du}{dr}\right]_{\text{CF}} + \left\{\frac{2}{r} + \frac{1}{r^2(1-\frac{2}{r})}\right\}}{\frac{1}{c_s} + \frac{c_s}{\gamma-(1+c_s^2)}} \quad (53)$$

The explicit expression for the velocity space gradient comes out to be

$$\left[\frac{du}{dr}\right]_{\text{CF}} = \frac{c_s^2 \left(\frac{2}{r} + \frac{1}{r^2(1-\frac{2}{r})}\right) - f_2(r, \lambda)}{\frac{u}{1-u^2} (1 - c_s^2) - \frac{c_s^2}{u}} \quad (54)$$

The critical point conditions are calculated as

$$\left[u = c_s\right]_{r_c}, \quad [c_s]_{r_c} = \sqrt{\frac{f_2(r_c, \lambda)}{\frac{2}{r_c} + \frac{1}{r_c^2(1-\frac{2}{r_c})}}} \Big|_{\text{CF}} \quad (55)$$

To compute the numerical value(s) of the critical point(s), one needs to substitute the critical point condition into the expression for \mathcal{E} to obtain an algebraic polynomial of the form $\mathcal{E} - f(r_c, \lambda, \gamma) = 0$, which is to be solved for r_c for initial boundary conditions described by the astrophysically relevant values of $[\mathcal{E}, \lambda, \gamma]$. For conical flow, $\mathcal{E} - f(r_c, \lambda, \gamma) = 0$ provides a polynomial in r_c of eleventh degree. The explicit expression for such polynomial is provided in the appendix.

Polynomials of degree higher than four can not be solved analytically. However, the number of roots of such equations lying between infinity and the event horizons can be estimated analytically using the generalized Sturm sequence algorithm.⁸⁷

The expressions for the critical values of (du/dr) and (dc_s/dr) have been provided in the appendix.

The expression for the acoustic surface gravity can be obtained as

$$\kappa_{\text{Adiabatic}}^{\text{Conical Flow}} = \left| \frac{r-2}{r^2(1-c_s^2)} \sqrt{r^2 - \lambda^2 \left(1 - \frac{2}{r}\right)} \left[\eta_1 \frac{du}{dr} + \sigma_2 \right] \right|_{r_c} \quad (56)$$

where

$$\sigma_2 = \left(\frac{\gamma-1}{2}\right) \left(\frac{\frac{2}{r} + \frac{1}{r^2(1-\frac{2}{r})}}{\frac{1}{u} + \frac{u}{\gamma-(1+u^2)}} \right) \quad (57)$$

6.1.3. Flow in hydrostatic equilibrium along the vertical direction

The radius dependent disc height is calculated as

$$H(r) = \frac{r^2 c_s}{\lambda} \sqrt{\frac{2(1-u^2)(1-\frac{\lambda^2}{r^2}(1-\frac{2}{r}))(\gamma-1)}{\gamma(1-\frac{2}{r})(\gamma-(1+c_s^2))}} \quad (58)$$

and the corresponding mass accretion rate comes out to be

$$\dot{M}_{VE} = 4\pi\rho \frac{uc_s r^{\frac{3}{2}}}{\lambda} \sqrt{\frac{2(\gamma-1)(r^3-\lambda^2(r-2))}{\gamma(\gamma-(1+c_s^2))}} \quad (59)$$

The entropy accretion rate is

$$[\dot{\Sigma}]_{VE} = \sqrt{\frac{2}{\gamma}} \left[\frac{\gamma-1}{\gamma-(1+c_s^2)} \right]^{\frac{\gamma+1}{2(\gamma-1)}} \frac{c_s^{\frac{\gamma+1}{\gamma-1}}}{\lambda} \sqrt{1-\frac{\lambda^2}{r^2}(1-\frac{2}{r})} (4\pi u r^3) \quad (60)$$

The relationship between du/dr and dc_s/dr is

$$\left[\frac{dc_s}{dr} \right]_{VE} = \frac{-c_s \{ \gamma - (1+c_s^2) \}}{\gamma+1} \left(\frac{1}{u} \left[\frac{du}{dr} \right]_{VE} + \frac{3}{r} + \frac{\lambda^2}{r^3} \left\{ \frac{1-\frac{2}{r}}{1-\frac{\lambda^2}{r^2}(1-\frac{2}{r})} \right\} \right) \quad (61)$$

The explicit expression for du/dr thus comes out to be

$$\left[\frac{du}{dr} \right]_{VE} = \frac{\frac{2c_s^2}{\gamma+1} f_1(r, \lambda) - f_2(r, \lambda)}{\frac{u}{1-u^2} - \frac{2c_s^2}{(\gamma+1)u}} \quad (62)$$

The critical point condition

$$\left[u = \sqrt{\frac{1}{1+(\frac{\gamma+1}{2})(\frac{1}{c_s^2})}} \right]_{r_c} = \sqrt{\frac{f_2(r_c, \lambda)}{f_1(r_c, \lambda) + f_2(r_c, \lambda)}} \Big|_{VE} \quad (63)$$

indicates that critical surfaces are not the acoustic horizons for flow in vertical equilibrium since the value of the Mach number M at the critical point is found to be

$$M_c = \sqrt{\left(\frac{2}{\gamma+1} \right) \frac{f_1(r_c, \lambda)}{f_1(r_c, \lambda) + f_2(r_c, \lambda)}} \quad (64)$$

Unlike other flow models, to locate the radius of the acoustic horizon r_h for flow in vertical equilibrium, one needs to integrate the flow equations from the critical point upto the radial distance where Mach number becomes unity.

The location of the critical point can be obtained by solving an 8th degree polynomial equation, explicit expression of which is provided in the appendix. The expression for critical velocity gradients are also provided in the appendix.

The acoustic surface gravity can be calculated as

$$\kappa_{\text{Adiabatic}}^{\text{Vertical Equilibrium}} = \left| \frac{r-2}{r^2(1-c_s^2)} \sqrt{r^2-\lambda^2 \left(1-\frac{2}{r} \right)} \left[\eta_3 \frac{du}{dr} + \sigma_3 \right] \right|_{r_s} \quad (65)$$

where r_s is the sonic point which is to be obtained by integrating the flow equations from the corresponding critical points, and

$$\eta_3 = 1 + \frac{c_s}{u} \left(\frac{\gamma - (1 + c_s^2)}{\gamma + 1} \right), \quad \sigma_3 = \frac{c_s f_1 (\gamma - (1 + c_s^2))}{\gamma + 1} \quad (66)$$

6.2. Isothermal accretion

As is understood, the expression for the mass accretion rate for constant height and conical flow model for isothermal accretion will exactly be the same as those obtained for the adiabatic flow since the flow thickness does not depend on γ . For accretion in vertical equilibrium, however, the flow thickness will be different for two different equation of states and hence the corresponding mass accretion rate for the isothermal flow will also be different from its polytropic counterpart

$$[\dot{M}]_{\text{VE}}^{\text{Isothermal}} = 4\pi\rho \frac{r^{\frac{3}{2}} u c_s}{\lambda} \sqrt{2(r^3 - (r-2)\lambda^2)} \quad (67)$$

The corresponding (advective) velocity (space) gradients are obtained as

$$\left[\frac{du}{dr} \right]_{\text{CH}}^{\text{Isothermal}} = \frac{(2r^3 - 2(r-2)^2\lambda^2 + (1-r)(2r^3 + 4\lambda^2 - 2r\lambda^2)c_s^2)u(u^2 - 1)}{(2-r)r(-2r^3 - 4\lambda^2 + 2r\lambda^2)(u^2 - c_s^2)} \quad (68)$$

$$\left[\frac{du}{dr} \right]_{\text{CF}}^{\text{Isothermal}} = \frac{\{2r^3 - 2(r-2)^2\lambda^2 + (3-2r)(2r^3 + 4\lambda^2 - 2r\lambda^2)c_s^2\}u(u^2 - 1)}{(2-r)r(-2r^3 - 4\lambda^2 + 2r\lambda^2)(u^2 - c_s^2)} \quad (69)$$

$$\left[\frac{du}{dr} \right]_{\text{VE}}^{\text{Isothermal}} = \frac{[r^3 - (r-2)^2\lambda^2 + (2-r)(3r^3 + 3\lambda^2 - 2r\lambda^2)c_s^2]u(u^2 - 1)}{\frac{1}{2}r(r-2)(-2r^3 - 4\lambda^2 + 2r\lambda^2)[c_s^2 - (1 + c_s^2)u^2]} \quad (70)$$

In the appendix, we describe how one can obtain the critical point condition, the location of the sonic horizon(s), and the value of the respective quantities (required to estimate κ for isothermal flow) evaluated on such horizons.

A two parameter set $[T, \lambda]$ is to be provided to calculate the location of the critical points *completely analytically* (unlike the polytropic flow where the number of critical points could be computed analytically but not their locations). One interesting point to note is that unlike the accretion flow under the post Newtonian pseudo-Schwarzschild potentials (as derived in¹⁵), for complete general relativistic flow the critical surface does not coincide with the acoustic horizon for flow in vertical equilibrium even for isothermal accretion. Using the values of $\left[u, \frac{du}{dr} \right]_{r_h}^c$ as derived

^cFor isothermal flow, the sound speed remains constant for all values of $2 < r < \infty$.

in the appendix, we derive the corresponding expressions for the acoustic surface gravities for three different flow models for isothermal accretion

$$\kappa_{\text{Isothermal}}^{\text{Constant Height}} = \left| \frac{r-2}{r^2(1-c_s^2)} \sqrt{r^2 - \lambda^2 \left(1 - \frac{2}{r}\right)} \left(\frac{du}{dr} \right) \right|_{r_c} \quad (71)$$

$$\kappa_{\text{Isothermal}}^{\text{Conical Flow}} = \left| \frac{r-2}{r^2(1-c_s^2)} \sqrt{r^2 - \lambda^2 \left(1 - \frac{2}{r}\right)} \left(\frac{du}{dr} \right) \right|_{r_c} \quad (72)$$

$$\kappa_{\text{Isothermal}}^{\text{Vertical Equilibrium}} = \left| \frac{r-2}{r^2(1-c_s^2)} \sqrt{r^2 - \lambda^2 \left(1 - \frac{2}{r}\right)} \left(\frac{du}{dr} \right) \right|_{r_s} \quad (73)$$

where r_s is the sonic point which is to be obtained by integrating the flow equations from the corresponding critical point.

7. Dependence of acoustic surface gravity on flow geometry – Polytropic accretion

In this section we will manifest how the geometric configuration of the non self-gravitating axially symmetric stationary background flow in a Schwarzschild metric influences the computation of the acoustic surface gravity for polytropic accretion onto astrophysical black holes. We first construct the parameter space determined by the initial boundary conditions to show the parameter dependence of the multi-critical flow behavior, and then will describe how one can pick certain regions of $[\mathcal{E}, \lambda, \gamma]$ space for which mono-transonic accretion is possible for all three different geometric configurations.

7.1. The parameter space classification

The critical point(s) are obtained once $[\mathcal{E}, \lambda, \gamma]$ is specified. A three dimensional parameter space spanned by $[\mathcal{E}, \lambda, \gamma]$ and bounded by an astrophysically relevant range $[1 < \mathcal{E} < 2, 0 < \lambda \leq 4, 4/3 \leq \gamma \leq 5/3]$, can thus be explored to understand the dependence of the multi-critical behavior on initial boundary conditions.

For the sake of convenience, a two dimensional projection of such a three dimensional parameter space will be analyzed. 3C_2 allowed combinations of such projections are available. In this work, we prefer to project the $[\mathcal{E}, \lambda, \gamma]$ space on a $[\mathcal{E}, \lambda]$ plane by keeping the adiabatic constant fixed to the value $\gamma = 4/3$. Although such $[\mathcal{E}, \lambda]$ projections can be studied for any other values lying in the range $4/3 \leq \gamma \leq 5/3$ as well.

In figure 1, we study the $\mathcal{E}-\lambda$ plane for three different flow geometries. Variation of $\mathcal{E}-\lambda$ branches for flow in hydrostatic equilibrium along the vertical direction, conical flow and flow with constant thickness are represented by solid red lines, dashed green lines, and dotted blue lines, respectively. Hereafter, we will follow the aforementioned color scheme to show results corresponding to the flow geometries

discussed above. For flow with constant height, $A_1A_2A_3A_4$ represents the region of $[\mathcal{E}, \lambda]$ for which eq. (40) along with the corresponding critical point conditions provides three real positive roots lying outside the gravitational horizon. For region $A_1A_2A_3$, one finds $\dot{\mathcal{E}}_{\text{inner}} > \dot{\mathcal{E}}_{\text{outer}}$ and accretion is multi-critical. A subspace of $A_1A_2A_3$ allows shock formation. Such a subspace provides true multi-transonic accretion where the stationary transonic solution passing through the outer sonic point joins with the stationary transonic solution constructed through the inner sonic point through a discontinuous energy preserving shock of Rankine-Hugoniot type. Such shocked multi-transonic solution contains two smooth transonic (from sub to super) transitions at two regular sonic points (of saddle type) and a discontinuous transition (from super to sub) at the shock location.

On the other hand, the region $A_1A_3A_4$ represents the subset of $[\mathcal{E}, \lambda, \gamma]_{\text{mc}}$ (where ‘mc’ stands for ‘multi-critical’) for which $\dot{\mathcal{E}}_{\text{inner}} < \dot{\mathcal{E}}_{\text{outer}}$ and hence incoming flow can have only one critical point of saddle type and the background flow possesses one acoustic horizon at the inner saddle type sonic point. The boundary A_1A_3 between these two regions represents the value of $[\mathcal{E}, \lambda, \gamma]$ for which multi-critical accretion is characterized by $\dot{\mathcal{E}}_{\text{inner}} = \dot{\mathcal{E}}_{\text{outer}}$ and hence the transonic solutions passing through the inner and the outer sonic points are completely degenerate, leading to the formation of a heteroclinic orbit^d on the phase portrait. Such flow configuration can not be used to study the analogue properties as we believe since it does not have uniqueness in forming the acoustic horizons. Such flow pattern is subjected to instability and turbulence as well.⁴⁸

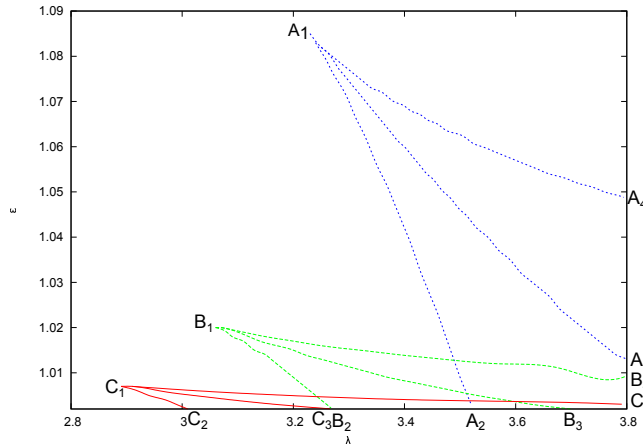


Fig. 1. $\mathcal{E}-\lambda$ plane for three different flow geometries for adiabatic accretion for fixed value of $\gamma = 4/3$. Variation of $\mathcal{E}-\lambda$ branches for flow in hydrostatic equilibrium along the vertical direction, conical flow and flow with constant thickness are represented by solid red lines, dashed green lines, and dotted blue lines, respectively. See section 7.1 for further details about the parameter space classification.

Similar analysis can be carried out for other two flow geometries. $B_1B_2B_3B_4$ and $C_1C_2C_3C_4$ represents $[\mathcal{E}, \lambda, \gamma]_{\text{mc}} \subset [\mathcal{E}, \lambda, \gamma]$ for the quasi-spherical conical flow and

^dHeteroclinic orbits are the trajectories defined on a phase portrait which connects two different saddle type critical points. Integral solution configuration on phase portrait characterized by heteroclinic orbits are topologically unstable.⁶⁹⁻⁷¹

Fig. 2.

For $[\mathcal{E} = 1.12, \gamma = 4/3]$, variation of the location of the acoustic horizons as a function of the flow angular momentum λ for stationary mono-transonic adiabatic accretion passing through the inner sonic point r_s for the three different geometric configurations of the flow considered in this work. $r_s - \lambda$ curves for flow in hydrostatic equilibrium along the vertical direction, conical flow and flow with constant thickness are represented by solid red lines, dashed green lines, and dotted blue lines, respectively.

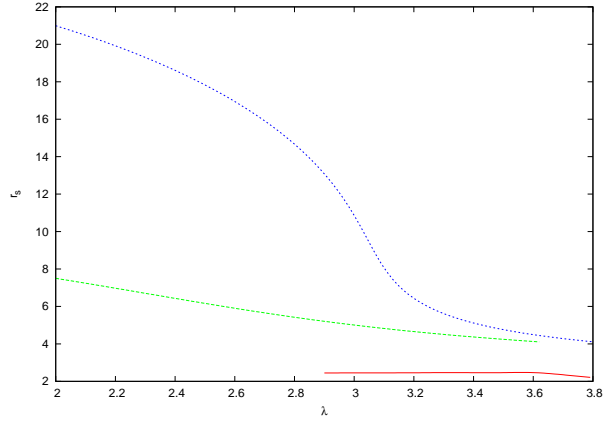


Fig. 3. For the same initial boundary conditions used to obtain figure 2, variation of acoustic surface gravity κ with the flow angular momentum λ for stationary mono-transonic adiabatic accretion passing through the inner sonic point r_s for the three different geometric configurations of the flow considered in this work. $\kappa - \lambda$ curves for flow in hydrostatic equilibrium along the vertical direction, conical flow and flow with constant thickness are represented by solid red lines, dashed green lines, and dotted blue lines, respectively.

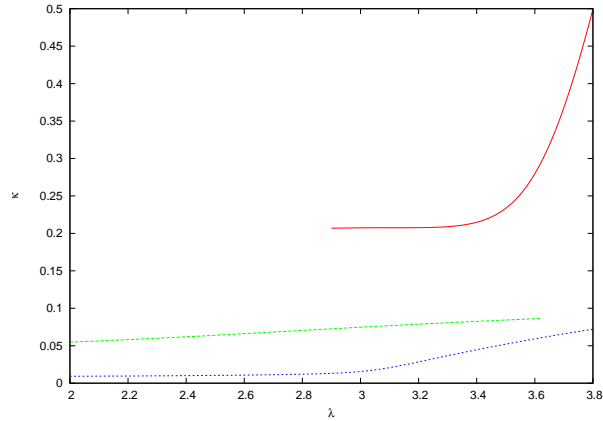
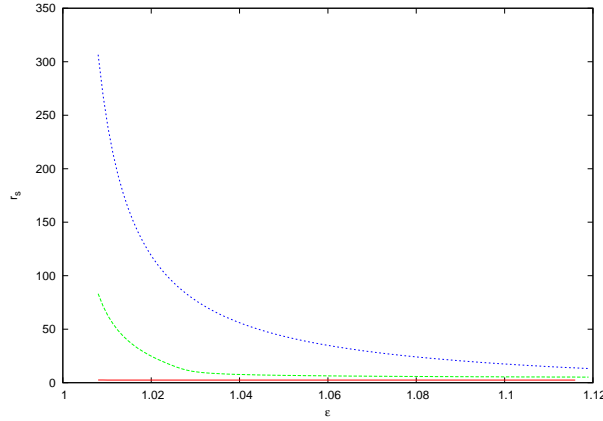


Fig. 4.

For $[\lambda = 2.89, \gamma = 4/3]$, variation of the location of the acoustic horizons as a function of the specific energy of the flow \mathcal{E} for stationary mono-transonic adiabatic accretion passing through the inner sonic point r_s for the three different geometric configurations of the flow considered in this work. $r_s - \mathcal{E}$ curves for flow in hydrostatic equilibrium along the vertical direction, conical flow and flow with constant thickness are represented by solid red lines, dashed green lines, and dotted blue lines, respectively.



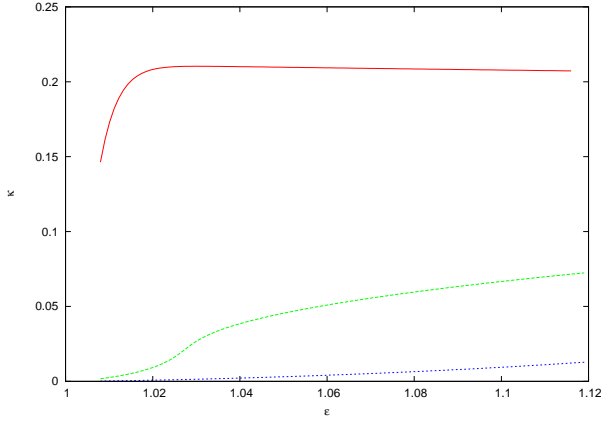


Fig. 5. For the same initial boundary conditions used to obtain figure 4, variation of acoustic surface gravity κ with the specific energy of the flow \mathcal{E} for stationary monotonsonic adiabatic accretion passing through the inner sonic point r_s for the three different geometric configurations of the flow considered in this work. $\kappa - \mathcal{E}$ curves for flow in hydrostatic equilibrium along the vertical direction, conical flow and flow with constant thickness are represented by solid red lines, dashed green lines, and dotted blue lines, respectively.

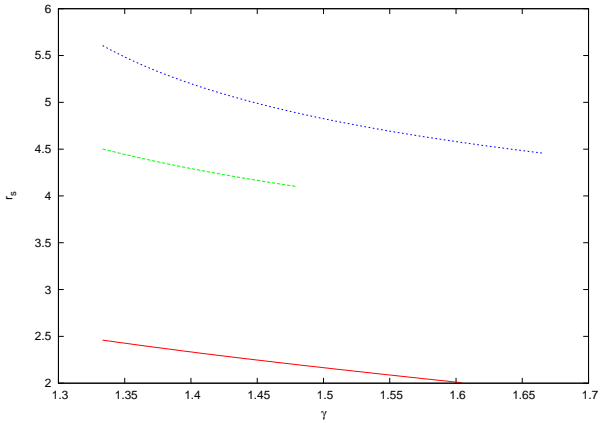


Fig. 6. For $[\mathcal{E} = 1.12, \lambda = 3.3]$, variation of the location of the acoustic horizons as a function of the adiabatic index γ for stationary monotonsonic adiabatic accretion passing through the inner sonic point r_s for the three different geometric configurations of the flow considered in this work. $r_s - \gamma$ curves for flow in hydrostatic equilibrium along the vertical direction, conical flow and flow with constant thickness are represented by solid red lines, dashed green lines, and dotted blue lines, respectively.

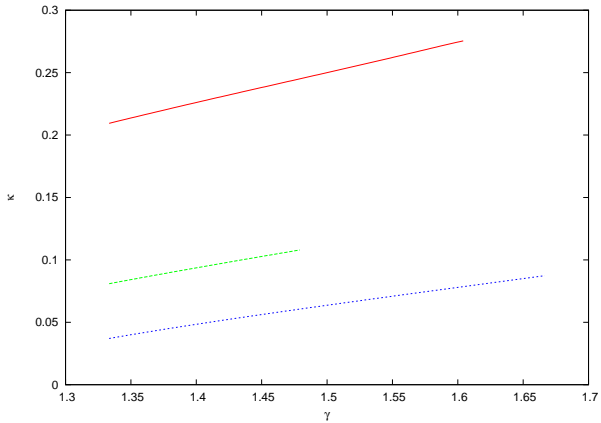


Fig. 7. For the same initial boundary conditions used to obtain figure 6, variation of acoustic surface gravity κ with the adiabatic index γ has been plotted for stationary monotonsonic adiabatic accretion passing through the inner sonic point r_s for the three different geometric configurations of the flow considered in this work. $\kappa - \gamma$ curves for flow in hydrostatic equilibrium along the vertical direction, conical flow and flow with constant thickness are represented by solid red lines, dashed green lines, and dotted blue lines, respectively.

for flow in vertical equilibrium, respectively. For $B_1B_2B_3B_4$, $B_1B_2B_3$ represents the multi-critical flow with $\dot{\mathcal{E}}_{\text{inner}} > \dot{\mathcal{E}}_{\text{outer}}$ and $B_1B_3B_4$ represents such region for $\dot{\mathcal{E}}_{\text{inner}} < \dot{\mathcal{E}}_{\text{outer}}$, B_1B_3 being the interface between them representing the values of $[\mathcal{E}, \lambda, \gamma]$ for which only the heteroclinic connections are obtained. Similar classifications can also be made for the region $C_1C_2C_3C_4$ as well.

We would like to pick a range of $[\mathcal{E}, \lambda, \gamma]$ for which all three flow configurations will provide mono-transonic accretion. Moreover, we are interested mainly in the stationary mono-transonic solutions passing through the inner sonic point since the acoustic surface gravity evaluated at the inner acoustic horizon is of the order of magnitude (upto about 10^5 or even higher) higher than the acoustic surface gravity evaluated at the outer acoustic horizon. In addition, the location of the outer acoustic horizon, and hence the value of the acoustic surface gravity evaluated on it, are not much sensitive to the variation of $[\mathcal{E}, \lambda, \gamma]$ compared to their counterparts corresponding to the inner acoustic horizon.

Out of the three parameters \mathcal{E} , λ and γ , we choose one parameter, say λ , to vary by keeping the values of $[\mathcal{E}, \gamma]$ fixed, for three different flow configurations for the mono-transonic flow through the inner acoustic horizon to obtain the $[\kappa - \lambda]$ variation. Three different $[\kappa - \lambda]$ variations for three different flow geometries will then be compared to examine the influence of the flow configuration on the value of the acoustic surface gravity. We perform the same operation for the other two parameters \mathcal{E} and λ , to obtain the $[\kappa - \mathcal{E}]$ and $[\kappa - \gamma]$ variations for three different flow geometries by keeping $[\lambda, \gamma]$ and $[\mathcal{E}, \lambda]$ invariant, respectively. Finally, we perform similar exercise for isothermal accretion of three different flow geometries to obtain and to mutually compare the $[\kappa - \lambda]$ and $[\kappa - T]$ variations, respectively.

7.2. Variation of κ with $[\mathcal{E}, \lambda, \gamma]$

In figure 2, for a fixed set of $[\mathcal{E} = 1.12, \gamma = 4/3]^e$, we plot the location of the inner type acoustic horizon (the inner sonic point r_s) as a function of the specific angular momentum λ of the flow for mono-transonic stationary accretion solution for three different flow geometries. It is observed that the location of the acoustic horizon anti-correlates with λ . This is somewhat obvious because for greater amount of rotational energy content of the flow, accretion starts with smaller advective velocity and has to approach very close to the event horizon to acquire the dynamical velocity sufficiently large to smoothly overcome the acoustic velocity.

For a specified initial boundary condition describing the flow, one observes

$$r_s^{\text{vertical}} < r_s^{\text{conical}} < r_s^{\text{constant height}} \quad (74)$$

This indicates that for the same set of $[\mathcal{E}, \lambda, \gamma]$, the acoustic horizon for accretion in hydrostatic equilibrium along the vertical direction forms at the closest proxim-

^eSuch a high value of \mathcal{E} ('hot' accretion) has been considered to ensure that mono-transonic stationary solution passing through the inner sonic point is obtained for all three different geometrical configurations of the axisymmetric matter considered in this work.

ity of the black hole event horizon and hence the relativistic acoustic geometry at the neighborhood of such acoustic horizons are subjected to considerably strong gravity space time. One thus intuitively concludes that among all three flow configurations considered in this work, the Hawking like effects may perhaps be more pronounced for axisymmetric background flow in hydrostatic equilibrium along the vertical direction. This intuitive conclusion is further supported by results represented in figure 3 where we have studied the variation of the acoustic surface gravity κ as a function of the flow angular momentum λ for the same set of initial boundary conditions as well as for the span of λ for which figure 2 has been obtained. For identical initial boundary conditions as determined by $[\mathcal{E}, \lambda, \gamma]$, one obtains

$$\kappa^{\text{vertical}} > \kappa^{\text{conical}} > \kappa^{\text{constant height}} \quad (75)$$

For a fixed value of $[\lambda = 2.89, \gamma = 4/3]$, the variation of the location of the inner acoustic horizons (the inner sonic points r_s) as a function of the specific flow energy \mathcal{E} is plotted in figure 4. r_s anti-co-relates with \mathcal{E} for obvious reasons. At a large distance away from the accretor, the total specific energy is essentially determined by the thermal energy of the flow, a large value of \mathcal{E} ('hot' accretion) corresponds to a high value of the sound speed c_s to begin with. The subsonic to the supersonic transition takes place quite close to the black hole where the bulk flow velocity (the advective velocity u) becomes large enough to overcome the sound speed. Once again, flow in vertical equilibrium produces the acoustic horizons located at a relatively stronger gravity region. The analogue effect should be more pronounced for such geometric configuration of the flow. Results presented in figure 5, where the acoustic surface gravity κ has been plotted as a function of the specific energy of the flow for the same set of $[\lambda, \gamma]$ used to draw figure 4, asserts such conclusion. For a fixed value of $[\mathcal{E} = 1.12, \lambda = 3.3]$, in figure 6 we find that the location of the acoustic horizon anti-correlates with γ and hence the acoustic surface gravity κ co-relates with γ as expected (as shown in figure 7). Similar result can be obtained for any set of $[\mathcal{E}, \lambda]$ for which monotonsonic stationary accretion passing through the inner type sonic point can be obtained for all three flow configurations considered in this work. Here too the acoustic surface gravity for accretion in hydrostatic equilibrium along the vertical direction is maximum (compared to the conical flow and flow with constant thickness) for the same set of initial boundary conditions. We thus obtain

$$\begin{aligned} r_s^{\text{vertical}} &< r_s^{\text{conical}} < r_s^{\text{constant height}} \\ \kappa^{\text{vertical}} &> \kappa^{\text{conical}} > \kappa^{\text{constant height}} \end{aligned} \quad (76)$$

here as well.

8. Dependence of acoustic surface gravity on flow geometry – Isothermal accretion

The $[T, \lambda]$ parameter space will first be constructed to manifest the multi-critical

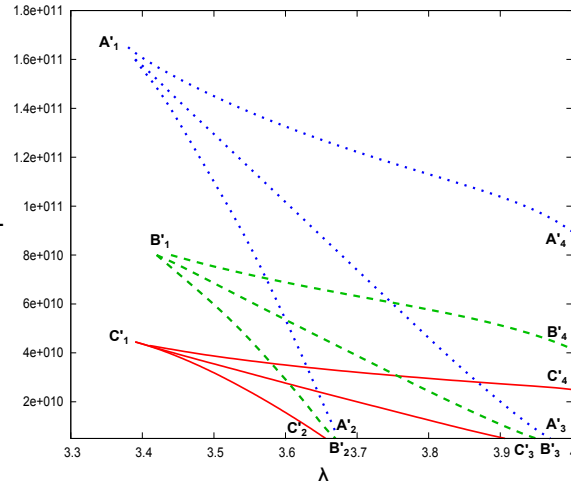
flow behavior. A certain subset of the entire $[T, \lambda]$ will then be chosen for which isothermal accretion in all three matter geometries will have mono-transonic solutions constructed through the inner sonic point.

8.1. The parameter space classification

Figure 8 depicts the parameter space division labeled following the scheme introduced in section 7.1. For constant height flow, conical flow and vertical equilibrium flow, $A'_1A'_2A'_3A'_4$, $B'_1B'_2B'_3B'_4$, and $C'_1C'_2C'_3C'_4$, represents the $[T, \lambda]$ regions for which eq. (95), eq. (97) and eq. (99) will provide three real physical roots located outside the gravitational horizon, respectively. It is to be noted that figure 8 can be obtained completely analytically solving the representative equations using the Ferrari's method.⁸⁵

Similar to the polytropic accretion, the wedge shaped region $[T, \lambda]_{mc}$, where 'mc' stands for 'multi-critical', has two subsections divided by a distinct boundary. However, unlike the entropy accretion rate \dot{M} for the polytropic flow, the first integral of motion ξ as defined in eq. (34) determines the characteristic features of various subspaces of $[T, \lambda]_{mc}$. For constant height flow, $A'_1A'_2A'_3A'_4$ region is subdivided into $A'_1A'_2A'_3$ for which $\xi_{in} > \xi_{out}$ and $A'_1A'_3A'_4$ for which $\xi_{in} < \xi_{out}$ with the boundary line $A'_1A'_3$ on which $\xi_{in} = \xi_{out}$. $[T, \lambda]_{A'_1A'_2A'_3}$ provides the multi-critical integral solutions for which the homoclinic orbit is constructed through the inner critical point whereas $[T, \lambda]_{A'_1A'_3A'_4}$ produces the multi-critical solution for which accretion is mono transonic and the corresponding homoclinic orbit is constructed through the outer critical point. $[T, \lambda]_{A'_1A'_3}$ provides the heteroclinic orbits for which one obtains degenerate accretion solutions.

Fig. 8. $T - \lambda$ plane for three different flow geometries for isothermal accretion. Variation of $T - \lambda$ branches for flow in hydrostatic equilibrium along the vertical direction, conical flow and flow with constant thickness are represented by solid red lines, dashed green lines, and dotted blue lines, respectively. See section 8.1 for further details about the parameter space classification.



For a certain subset of $[T, \lambda]_{A'_1A'_2A'_3} \in [T, \lambda]_{mc}$, temperature preserving shock may form to provide true multi-transonicity. Such stationary solutions contain two

acoustic black hole horizons at the inner and the outer sonic points and an acoustic white hole solution at the shock location. We, however, will not perform the shock finding analysis in the present work.

In a similar spirit, subdivisions in multi-critical parameter spaces for the conical and the vertical equilibrium can also be obtained.

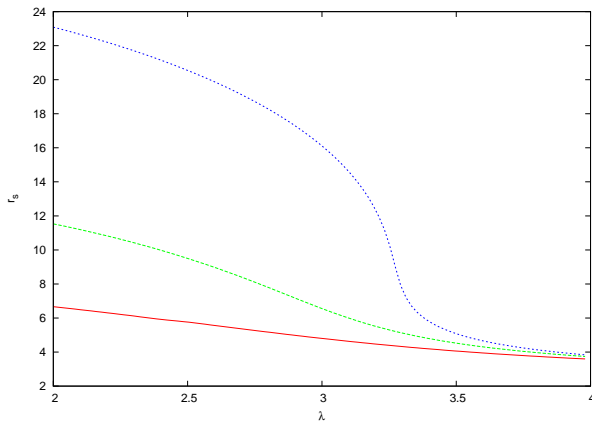


Fig. 9. For $T_{10} = 20.0$ (in units of 10^{10} K), variation of the location of the acoustic horizons as a function of the flow angular momentum λ for stationary mono-transonic isothermal accretion passing through the inner sonic point r_s for the three different geometric configurations of flow considered in this work. $r_s - \lambda$ curves for flow in hydrostatic equilibrium along the vertical direction, conical flow and flow with constant thickness are represented by solid red lines, dashed green lines, and dotted blue lines, respectively.

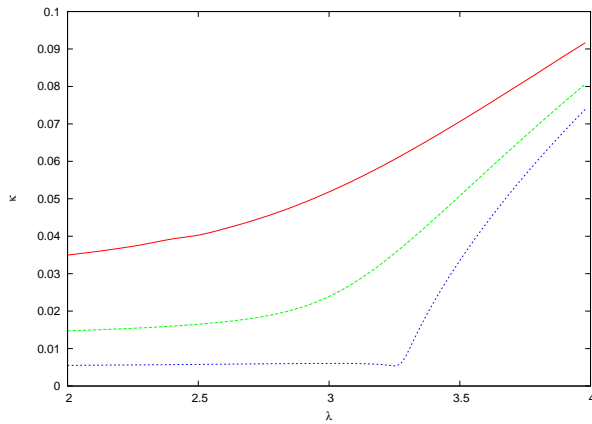


Fig. 10. For the same initial boundary conditions used to obtain figure 9, variation of acoustic surface gravity κ with the flow angular momentum λ for stationary mono-transonic isothermal accretion passing through the inner sonic point r_s for the three different geometric configurations of flow considered in this work. $\kappa - \lambda$ curves for flow in hydrostatic equilibrium along the vertical direction, conical flow and flow with constant thickness are represented by solid red lines, dashed green lines, and dotted blue lines, respectively.

8.2. Variation of κ with $[\lambda, T]$

In figure 9, we plot the variation of the location of the acoustic horizon (the inner sonic point r_s) with the constant specific angular momentum of the flow λ . The value of flow temperature T expressed in units of 10^{10} K and denoted by T_{10} has been fixed at 20.0, thus ensuring mono-transonic accretion for all three flow geometries. For obvious reasons (as described in section 7.2), r_s anti-correlates with

Fig. 11. For $\lambda = 3.3$, variation of the location of the acoustic horizon with the constant flow temperature T (in units of 10^{10} Kelvin and denoted as T_{10}) for stationary mono-transonic isothermal accretion passing through the inner sonic point r_s for the three different geometric configurations of the flow considered in this work. $r_s - T_{10}$ curves for flow in hydrostatic equilibrium along the vertical direction, conical flow and flow with constant thickness are represented by solid red lines, dashed green lines, and dotted blue lines, respectively.

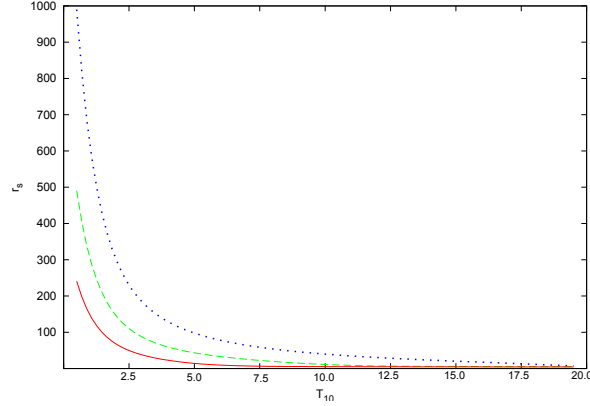
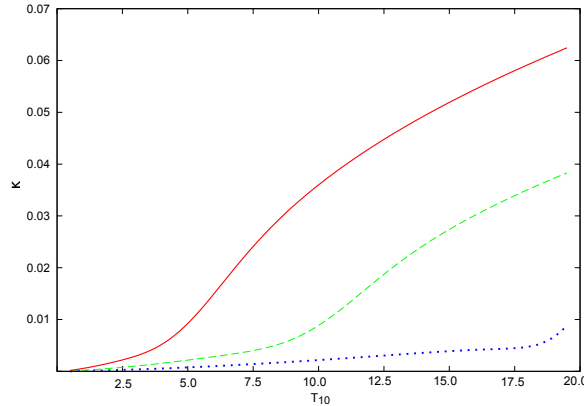


Fig. 12. For the same initial boundary conditions used to obtain figure 11, variation of acoustic surface gravity κ with the constant flow temperature T (in units of 10^{10} Kelvin and denoted as T_{10}) for stationary mono-transonic isothermal accretion passing through the inner sonic point r_s for three different geometric configuration of the flow considered in this work. $\kappa - T_{10}$ curves for flow in hydrostatic equilibrium along the vertical direction, conical flow and flow with constant thickness are represented by solid red lines, dashed green lines, and dotted blue lines, respectively.



λ . For accretion flow in hydrostatic equilibrium along the vertical direction, entire range of sonic points produced (for the domain of λ considered in this work) lie in the close proximity of the event horizon. This indicates that for the same set of initial boundary conditions describing the flow, the Hawking like effects will be maximally pronounced for such a flow model. Such a conclusion is further reinforced from results presented in figure 10 where we have plotted the acoustic surface gravity κ as a function of the flow angular momentum λ to obtain

$$\kappa^{\text{vertical}} > \kappa^{\text{conical}} > \kappa^{\text{constant height}} \quad (77)$$

Figure 11 represents the variation of the location of the acoustic horizon with constant flow temperature in units of T_{10} . Since the position independent sound speed $c_s \propto T^{\frac{1}{2}}$, the sonic point r_s anti-correlates with the flow temperature T . In figure 12 we plot the variation of the acoustic surface gravity κ as a function of T in units of T_{10} . Hotter flow produces larger value of the acoustic surface gravity κ .

9. Concluding remarks

For analogue models, the mass of the system itself can not determine the value of acoustic surface gravity (as well as the associated Hawking like temperature) since κ is obtained as a complicated non linear functional^f of the initial boundary conditions describing the flow profile. The same set of initial boundary conditions may provide significantly different phase portrait for integral stationary solutions for different geometric configurations of the background matter flow, and it is necessary to study the influence of the matter geometry on the determination of the corresponding relativistic acoustic geometry. In this work, we accomplish this task by studying the dependence of the value of κ on the geometric configurations of the background matter flow as well as on various astrophysically relevant initial boundary conditions governing such flow described by different thermodynamic equations of state. In this way we intend to provide a reference space spanned by fundamental accretion parameters to apprehend under which astrophysically relevant scenario the analogue effects will be pronounced.

As already mentioned in the introduction, we particularly emphasize on the geometric (sonic manifold) aspects of the system rather than the study of the field theoretic aspects and hence the analysis of the origin and the properties of the Hawking like radiation/temperature is beyond the scope of our present work.

We found that the Hawking like effects become more pronounced in the relatively stronger gravity region in the sense that irrespective of the equation of state as well as the initial boundary conditions, the acoustic surface gravity for stationary mono-transonic solutions assumes its maximum value when the acoustic horizons are formed at very close proximity of the black hole event horizon. Among all three geometric configurations of the background axisymmetric flow considered in this work, flow in hydrostatic equilibrium along the vertical direction produces the acoustic horizons of smallest radius and hence the corresponding surface gravity and the Hawking like temperature becomes maximum for such flow configuration. This is true for both the adiabatic as well as the isothermal accretion. It has also been observed that hotter flow (adiabatic flow parameterized by large value of \mathcal{E} or isothermal flow parameterized by high temperature) produces the larger value of the acoustic surface gravity since for such flow the inner type sonic points are formed very close to the black hole event horizon. Similar effects are observed for flow with large values of λ and γ . One thus concludes that relatively faster rotating hotter flows are responsible for maximizing the analogue effects for axisymmetric background flow in Schwarzschild metric.

As already clarified in the previous sections, non-universal features of Hawking like effects in dispersive media depends on the value of the space gradient of the background flow velocity as well as that of the speed of propagation of pertur-

^f κ is actually functions of $[u, c_s, du/dr, dc_s/dr]$ for adiabatic flow and $[u, c_s, du/dr]$ of isothermal flow. $[u, c_s, du/dr, dc_s/dr]_{\text{adia}}$ and $[u, c_s, du/dr]_{\text{iso}}$ are non linear functions of $[\mathcal{E}, \lambda, \gamma]_{\text{adia}}$ and $[T, \lambda]_{\text{iso}}$ respectively, and hence κ_{adia} and κ_{iso} are functionals of $[\mathcal{E}, \lambda, \gamma]_{\text{adia}}$ and $[T, \lambda]_{\text{iso}}$, respectively.

bation for fluid flow with position dependent sound speed. The aforementioned calibration space will also be useful to point out the relevance of certain astrophysical configurations to simulate the set up where such deviation can be maximum. This will certainly be useful to study the effect of gravity on the non-conventional classical features in Hawking like effects as is expected to be observed in the limit of a strong dispersion relation - no such work has been reported in the literature yet.

For adiabatic as well as for isothermal flows in hydrostatic equilibrium in the vertical direction, the critical point and the sonic points are found to be non-overlapping, and an integral solution of the flow equations are needed to obtain the location of the acoustic surface gravity. Note that whereas for the adiabatic flow it is true for pseudo-Schwarzschild accretion under the influence of the modified potentials, isothermal accretion within such modified Newtonian framework does not discriminate between a critical and a sonic point.¹⁷ It is, however, difficult to conclude anything about the universality of such phenomena since the corresponding expression for the flow thickness has been derived using a set of idealized assumptions. A more realistic flow thickness may be derived by employing the non-LTE radiative transfer^{80,81} or by taking recourse to the Grad-Shafranov equations for the MHD flow.⁸²⁻⁸⁴

In the present work, we concentrate on the calculation of the acoustic surface gravity κ for mono-transonic stationary integral accretion solutions constructed through the inner saddle type sonic points, and the multi-transonic flow solutions have not been considered. This, however, is not a limitation of our formalism. For multi-transonic accretion, the flow essentially passes through the inner sonic point anyway. We have also demonstrated that the value of κ evaluated at the inner acoustic horizon is significantly larger compared to its value evaluated at the outer acoustic horizons. Also κ for the inner acoustic horizon is far more sensitive to the initial boundary conditions. To understand the influence of the geometric configuration of matter on the sonic geometry, it is thus sufficient to study the mono-transonic flow through the inner acoustic horizon, at least for the present context as described above.

Study of the acoustic geometry for an entire shocked flow (with two solutions constructed through the outer and the inner sonic horizons connected by a discontinuous shock of practically zero thickness) might have other interesting consequences. The discriminant of the acoustic metric

$$\mathcal{D} \equiv G_{t\phi}^2 - G_{tt}G_{\phi\phi} \quad (78)$$

vanishes at the regular acoustic horizons. The notion of the sub (super) – to super (sub) sonic transition may be understood through the sign change of the discriminant. Stationary acoustic horizons are located at the corresponding radial distances where \mathcal{D} changes its sign. A regular smooth transition of $\mathcal{D} > 0 \rightarrow \mathcal{D} < 0$ kind represents an acoustic black hole and a discontinuity of $\mathcal{D} > 0 \rightarrow \mathcal{D} < 0$ type characterizes a shock, which actually can be considered as an acoustic white hole,

following the notion introduced in.⁸⁸ The major concern in dealing with a multi-transonic accretion is, however, the divergence of $[u_\perp, c_s]$ (and hence of their space gradients $\left[\frac{du_\perp}{dr}, \frac{dc_s}{dr}\right]$) at the shock location. Since

$$\kappa \equiv \kappa \left[u_\perp, c_s, \frac{du_\perp}{dr}, \frac{dc_s}{dr} \right], \quad (79)$$

the acoustic surface gravity also diverges in this case at the shock. If the analogue temperature is assumed to be directly proportional to the acoustic surface gravity, then such temperature can not be evaluated at shock as it seems. This apparently seems to be true for any discontinuity similar to the first order phase transition in general (shock transition considered in this paper shares the properties of a first order phase transition in thermodynamics). This is in accordance with the general remarks made in^{23,24} where the formalism for obtaining the Hawking like temperature fails to provide acceptable results for a considerably large value of the space gradient of the background flow velocity normal to the acoustic horizon (u_\perp – which is the advective velocity for the flow configurations considered in the present work).

There are, however, ample scopes for further critical discussion in this aspect. In the present work, irrotational inviscid flow with infinitely thin shock surface has been considered, leading to a sharp discontinuity in $[u_\perp, c_s]$ at the shock. For large scale relativistic astrophysical flows, however, the effect of viscosity and cosmic magnetic field may not be underestimated, resulting in the presence of various dissipative mechanisms (bulk heating and cooling for background flow, even if the steady flow remains a stable one) through the Comptonization, bremsstrahlung and synchrotron mechanism.^{89,90} It may even be subjected to the turbulent instabilities as well, and non linear perturbation may have non-negligible effects in studying the associated acoustic geometry. Effects of the Velikhov-Chandrasekhar⁹¹ or the Balbus-Hawley⁹² type magneto rotational instability (MRI) may become significant close to the gravitational horizon. Clearly, such flow can be considered neither inviscid nor irrotational, and will not allow the formation of zero-thickness standing shock – shock may still form but it will have finite thickness⁷⁵ with practically continuously (albeit quite steeply) varying flow variables (and their respective space gradients) at the shock. As a result, the discontinuity of $\left[u_\perp, c_s, \frac{du_\perp}{dr}, \frac{dc_s}{dr} \right]$ may be smeared out. However, they can possess large values resulting in a very large value of κ which can be considered as an astrophysical manifestation of the general result reported in.⁷⁹

For high viscous flow, even for steady hydrodynamic accretion, shock may not even form as an extreme case. That excludes the possibility of obtaining the aforementioned large value of κ for such background configuration. For shock-free multi-transonic flow, the stationary solutions constructed through the inner and the outer saddle type sonic points may join through a middle spiral type (instead of a centre type) critical point.

All such additional complexities (in the background flow configuration) mentioned above may bring the system into the risk of destroying the Lorentz invariance. Analytical modelling of such analogue systems may not be amenable. One has to take recourse to the large-scale numerical simulation to understand the dynamics of such a complex fluid configuration. From the analogue point of view, viscosity is likely to destroy the Lorentz invariance, and the assumptions behind constructing an acoustic geometry may not be quite consistent for such a case as mentioned above.

In our work, therefore, we consider only the inviscid flow. One of the significant effects of inclusion of the viscosity would be the reduction of the angular momentum. As we demonstrate in this work, the location of the acoustic horizon anti-correlates with λ . Weakly rotating flow makes the dynamical velocity gradient steeper leading to the conclusion that for viscous flow the acoustic horizons will be pushed further out from the black hole and the flow would become supersonic at a larger distance for the same set of other initial boundary conditions. The value of the acoustic surface gravity anti-correlates with the location of the acoustic horizon. A viscous transonic accretion disc is thus expected to produce lower value of κ compared to its inviscid counterpart.

As is obvious, we concentrate on stationary background solutions. Since transient phenomena are not quite uncommon in large scale accretion processes, it is thus important to ensure the stability of such stationary solutions - at least within a reasonable astrophysical time scale. One of our recent works⁹⁴ accomplished such task by perturbing the corresponding space-time dependent fluid dynamic equations governing the accretion process and by studying whether such perturbation converges to ensure the stability of the transonic solutions of the time independent part of the aforementioned fluid dynamic equations. Work presented in⁹⁴ ensures that the corresponding stationary integral transonic solutions are stable and demonstrates that the relativistic acoustic geometry emerges from such perturbation analysis, as well as it demonstrates that the acoustic metric obtained for such configurations is independent of the mode of perturbation, i.e., the sonic metric as well as κ remains invariant irrespective of whether the velocity potential or the mass accretion rate is perturbed using the linear perturbation technique. Such works may be considered as the dynamical treatment (to study the sonic geometry) corresponding to the stationary approach presented in our present work. In such works too, however, the shock related discontinuity can not be avoided (if shock forms in inviscid fluid) since the entire stability analysis scheme had been based on the linear perturbation analysis (where sound wave is defined as a small amplitude linear perturbation, following the general convention).

There are, however, recently published works on the possibility of calculation of the Hawking like temperature for flow with discontinuities. For dilute Bose-Einstein condensates with a step like horizon, microscopic Bogoliubov theory has been applied⁹⁵ to obtain a closed form analytical expression for the spectral distri-

bution of the analogue radiation, even if the corresponding surface gravity diverges because of the discontinuous profile. Expression for the Hawking like temperature could not be obtained but the spectrum had been predicted to be a thermal one for such case. Later on, a series of works by Finazzi and his collaborators^{96,97} used non-linear dispersion relation to obtain the analogue temperature for Bose-Einstein condensates (and claimed that the result holds good for more general kind of flow as well), even if the profile contains discontinuity. In their work, a critical length had been defined as a function of the healing length ζ (originally defined by² and later on re-interpreted by⁹⁸ in the relevant context) and the acoustic surface gravity κ . The gradient of the dynamical velocity was then computed over the aforementioned critical length scale across the horizon to obtain the emergent spectrum. Even if the analogue temperature differs considerably from the Hawking one, the corresponding flux still comes out to be thermal.

We are, however, not sure whether the analogue temperature can be found out at the shock location for the flow profile we consider. Being an inviscid flow, the shock is infinitely thin, and the discontinuity resembles a delta function, which rules out the possibility of any ‘smooth averaging’ over such discontinuity (had it been the case that the shock would have finite thickness, such an averaging procedure could perhaps be relevant in the present context). Also our perturbation analysis is linear and no leading term with higher order perturbation is considered while obtaining the corresponding wave equation (for the propagation of the perturbation) and the associated acoustic metric element $G_{\mu\nu}$. Hence application of the methodology developed in^{96,97} in our work to compute the corresponding analogue temperature and the associated spectra at the shock would be considerably involved and is, unfortunately, beyond the scope of the present paper. Nevertheless, it will really be interesting to see whether such a methodology could be adopted for the shocked flow configuration considered here since it would open up an unique possibility of obtaining very large (and hence, observationally detectable) analogue temperature at the shock. We plan to perform such task in future for astrophysical flows with finite shock thickness.

Our present work deals with accretion onto non-rotating black holes. The hypothesis that some of the supermassive black holes and the stellar mass black holes powering the active galactic nuclei and the galactic microquasars, respectively, possess non-zero values of the spin angular momentum in reality, has gained widespread acceptance in recent times.^{99–118} The black hole spin plays a deterministic role in influencing various characteristic dynamical and spectral features of accretion and related phenomena in the characteristic metric. We thus feel that it is imperative to study the influence of the black hole spin angular momentum on the emergence of the relativistic sonic geometry for black hole accretion in the Kerr metric. In our next work we shall report how the $\kappa - a$ (a being the Kerr parameter) profile differs for various flow geometries and equations of state. This will greatly help to understand how the actual black hole metric influences the properties of

the emergent acoustic metric. In addition, from recent theoretical and observational findings, the relevance of the counter-rotating accretion in black hole astrophysics is being increasingly evident.^{108–110, 119} It is thus instructive to study whether the characteristic features of the various $\kappa - a$ profiles manifest any discrimination between a prograde and a retrograde background flow.

10. Appendices

10.1. Determination of the location of the sonic horizon(s) and the critical velocity gradients at such horizons – Polytropic accretion.

In this section we shall demonstrate how one can obtain an algebraic polynomial in r_c , the critical point of the flow, and how the computation of the location of the acoustic horizons r_h follows from such procedure. We then obtain the values of the dynamical velocity (radial advective velocity on the equatorial plane) and the sonic velocity (speed of propagation of the embedded linear perturbation), as well as their space gradients, evaluated on the acoustic horizon r_h . This completes the exact estimation of the value of the acoustic surface gravity κ since

$$\kappa \equiv \kappa \left[u, c_s, \frac{du}{dr}, \frac{dc_s}{dr} \right]_{r_h} \quad (80)$$

as has been shown in eq. (3).

The total specific energy first integral of motion

$$\mathcal{E} = \frac{\gamma - 1}{(\gamma - (1 + c_s^2))} \sqrt{\frac{(1 - \frac{2}{r})}{(1 - \frac{\lambda^2}{r^2})(1 - \frac{2}{r})(1 - u^2)}} \quad (81)$$

remains conserved for every r , including r_c (and r_h , if $r_h \neq r_c$, we shall discuss such cases in detail), for polytropic accretion. For the constant height flow, critical point condition comes out to be (see eq. 46)

$$[u = c_s]_{r_c} = \sqrt{\frac{f_2(r_c, \lambda)}{\frac{1}{r_c} + \frac{1}{r_c^2(1 - \frac{2}{r_c})}}} \quad (82)$$

where $f_2(r_c, \lambda)$ are obtained by substituting $r = r_c$ in the expression provided by eq. (45a).

Substitution of the value of u and c_s evaluated at the critical point (expressed through the eq.(82)) in eq. (81) provides the following 11th degree algebraic polynomial equation in r_c

$$a_0 + a_1 r_c + a_2 r_c^2 + a_3 r_c^3 + a_4 r_c^4 + a_5 r_c^5 + a_6 r_c^6 + a_7 r_c^7 + a_8 r_c^8 + a_9 r_c^9 + a_{10} r_c^{10} + a_{11} r_c^{11} = 0 \quad (83)$$

where, the coefficients a_i are given by

$$\begin{aligned}
a_0 &= 4(\gamma - 3)^2 \lambda^6 \mathcal{E}^2 \\
a_1 &= -4(3\gamma^2 - 16\gamma + 21) \lambda^6 \mathcal{E}^2 \\
a_2 &= \lambda^4 \left((13\gamma^2 - 62\gamma + 73) \lambda^2 \mathcal{E}^2 - 4(\gamma - 1)^2 \right) \\
a_3 &= 2\lambda^4 \left(2(4(\gamma - 1)^2 + 3(\gamma - 3)\mathcal{E}^2) - (3\gamma^2 - 13\gamma + 14) \lambda^2 \mathcal{E}^2 \right) \\
a_4 &= \lambda^4 \left(-25(\gamma - 1)^2 + 2(\gamma^2 - 17\gamma + 36) \mathcal{E}^2 + (\gamma - 2)^2 \lambda^2 \mathcal{E}^2 \right) \\
a_5 &= \lambda^2 \left(-4(\gamma - 1)^2 - \lambda^2 \left((5\gamma^2 - 38\gamma + 59) \mathcal{E}^2 - 19(\gamma - 1)^2 \right) \right) \\
a_6 &= \lambda^2 \left(\lambda^2 \left(4(\gamma^2 - 5\gamma + 6) \mathcal{E}^2 - 7(\gamma - 1)^2 \right) + \gamma^2 (14 - 3\mathcal{E}^2) + 4\gamma (3\mathcal{E}^2 - 7) + 14 \right) \\
a_7 &= \lambda^2 \left(2(2\gamma^2 - 7\gamma + 3) \mathcal{E}^2 - 9(\gamma - 1)^2 - \lambda^2 \left((\gamma - 2)^2 \mathcal{E}^2 - (\gamma - 1)^2 \right) \right) \\
a_8 &= -(\gamma - 1)^2 - \lambda^2 \left((7\gamma^2 - 22\gamma + 13) \mathcal{E}^2 - 10(\gamma - 1)^2 \right) \\
a_9 &= -6\gamma + \gamma^2 \left(-(\mathcal{E}^2 - 3) \right) + 2(\gamma - 1) \lambda^2 \left(-\gamma + (\gamma - 2) \mathcal{E}^2 + 1 \right) + 3 \\
a_{10} &= (\gamma - 1) \left(\gamma (2\mathcal{E}^2 - 3) + 3 \right) \\
a_{11} &= (\gamma - 1)^2 (1 - \mathcal{E}^2)
\end{aligned} \tag{84}$$

A specific choice of the initial boundary conditions governing the flow and specified by astrophysically relevant values of $[\mathcal{E}, \lambda, \gamma]$ is required to solve the above equation for r_c . Eq. (82) implies that the critical surfaces are isomorphic with the sonic surfaces, and hence r_c and r_h is identical. This requires that an acceptable root (of the aforementioned polynomial) will be real, positive and should lie outside the gravitational horizon (located at $r = 2$ in the system of units used in the present work).

For conical flow, the critical point condition

$$[u = c_s]_{r_c} = \sqrt{\frac{f_2(r_c, \lambda)}{\frac{2}{r_c} + \frac{1}{r_c^2(1 - \frac{2}{r_c})}}}, \tag{85}$$

implies that $r_c = r_h$, and when substituted in eq. (81), provides the following 11th polynomial equation

$$a_0 + a_1 r_c + a_2 r_c^2 + a_3 r_c^3 + a_4 r_c^4 + a_5 r_c^5 + a_6 r_c^6 + a_7 r_c^7 + a_8 r_c^8 + a_9 r_c^9 + a_{10} r_c^{10} + a_{11} r_c^{11} = 0 \tag{86}$$

40 *Tarafdar & Das*

where the coefficients a_i are found to be

$$\begin{aligned}
 a_0 &= -4\mathcal{E}^2(5 - 3\gamma)^2\lambda^6 \\
 a_1 &= 8\mathcal{E}^2(40 - 49\gamma + 15\gamma^2)\lambda^6 \\
 a_2 &= -\lambda^4(108 + 401\mathcal{E}^2\lambda^2 + \gamma^2(108 + 157\mathcal{E}^2\lambda^2) - 2\gamma(108 + 251\mathcal{E}^2\lambda^2)) \\
 a_3 &= \lambda^4(324(-1 + \gamma)^2 + \mathcal{E}^2(-240 + 247\lambda^2 - 4\gamma(-81 + 79\lambda^2) + \gamma^2(-108 + 101\lambda^2))) \\
 a_4 &= \lambda^4(-387(-1 + \gamma)^2 + \mathcal{E}^2(564 - 75\lambda^2 + \gamma^2(270 - 32\lambda^2) + \gamma(-786 + 98\lambda^2))) \\
 a_5 &= \lambda^2(-108 + (230 - 502\mathcal{E}^2)\lambda^2 + 9\mathcal{E}^2\lambda^4 + 2\gamma^2(-54 + (115 - 126\mathcal{E}^2)\lambda^2 + 2\mathcal{E}^2\lambda^4)) \\
 a_6 &= \lambda^2(-2(-1 + \gamma)^2(-135 + 34\lambda^2) + \mathcal{E}^2(-84 + 200\lambda^2 + \gamma(180 - 290\lambda^2) + \gamma^2(-81 + 104\lambda^2))) \\
 a_7 &= \lambda^2(4(-1 + \gamma)^2(-63 + 2\lambda^2) + \mathcal{E}^2(\gamma^2(153 - 16\lambda^2) - 30(-6 + \lambda^2) + 4\gamma(-87 + 11\lambda^2))) \\
 a_8 &= -27 - 4(-26 + 31\mathcal{E}^2)\lambda^2 + \gamma^2(-27 + (104 - 96\mathcal{E}^2)\lambda^2) + \gamma(54 + 16(-13 + 14\mathcal{E}^2)\lambda^2) \\
 a_9 &= 2(-(-1 + \gamma)^2(-27 + 8\lambda^2) + \mathcal{E}^2(-4 + 14\lambda^2 + \gamma(12 - 24\lambda^2) + \gamma^2(-9 + 10\lambda^2))) \\
 a_{10} &= 4(-1 + \gamma)(9 - 9\gamma + \mathcal{E}^2(-4 + 6\gamma)) \\
 a_{11} &= -8(-1 + \mathcal{E}^2)(-1 + \gamma)^2
 \end{aligned}$$

For flow in vertical equilibrium, the critical point condition

$$\left[u = \sqrt{\frac{1}{1 + (\frac{\gamma+1}{2})(\frac{1}{c_s^2})}} \right]_{r_c} = \sqrt{\frac{f_2(r_c, \lambda)}{f_1(r_c, \lambda) + f_2(r_c, \lambda)}} \quad (87)$$

indicates that the critical points and the sonic points are not located at the same radial distance, and the value of flow variables and their space gradients on the sonic horizons are to be obtained by integrating the flow equation using the critical flow variables (as well as their gradients). In eq. (87), $f_1(r_c, \lambda)$ is obtained by putting $r = r_c$ in eq. (45b). Substituting the values of the critical velocities (as obtained through eq. (87) in eq. (81), the following 8th degree polynomial equation in r_c is obtained

$$a_0 + a_1 r_c + a_2 r_c^2 + a_3 r_c^3 + a_4 r_c^4 + a_5 r_c^5 + a_6 r_c^6 + a_7 r_c^7 + a_8 r_c^8 = 0 \quad (88)$$

where the coefficients a_i are found to be

$$\begin{aligned}
 a_0 &= 64(-2 + \gamma)^2 \mathcal{E}^2 \lambda^4 \\
 a_1 &= -32(18 - 19\gamma + 5\gamma^2) \mathcal{E}^2 \lambda^4 \\
 a_2 &= 4\lambda^2((121 - 134\gamma + 37\gamma^2) \mathcal{E}^2 \lambda^2 + 60(-1 + \gamma)^2) \\
 a_3 &= 4\lambda^2((-45 + 52\gamma - 15\gamma^2) \mathcal{E}^2 \lambda^2 + 4(-34 + 22\mathcal{E}^2 + \gamma(68 - 37\mathcal{E}^2) + \gamma^2(-34 + 13\mathcal{E}^2))) \\
 a_4 &= \lambda^2((5 - 3\gamma)^2 \mathcal{E}^2 \lambda^2 - 4(-115 + 147\mathcal{E}^2 + \gamma(230 - 244\mathcal{E}^2) + \gamma^2(-115 + 89\mathcal{E}^2))) \\
 a_5 &= -2(-60(-1 + \gamma)^2 + (86 - 163\mathcal{E}^2 + \gamma^2(86 - 99\mathcal{E}^2) + 2\gamma(-86 + 133\mathcal{E}^2))\lambda^2 - 60(-1 + \gamma)^2) \\
 a_6 &= (-12(-1 + \gamma)(2 - 5\mathcal{E}^2 + \gamma(-2 + 3\mathcal{E}^2))\lambda^2 + (-384 + 121\mathcal{E}^2 + \gamma(768 - 286\mathcal{E}^2) + \gamma^2(-384 + 169\mathcal{E}^2))) \\
 a_7 &= -12(-1 + \gamma)(17 - 11\mathcal{E}^2 + \gamma(-17 + 13\mathcal{E}^2)) \\
 a_8 &= 36(-1 + \gamma)^2(-1 + \mathcal{E}^2)
 \end{aligned}$$

One needs to realize that unlike the other two flow models, it is necessary but not sufficient to have a root for the above equation as $r_c > 2$, since we need $r_h > 2$ and $r_h < r_c$ always.

Space gradient of advective velocity for various flow models can be obtained as

$$\left[\left(\frac{du}{dr} \right)_{r_c} \right]_i = \left[-\frac{\alpha_i}{2\Gamma_i} + \frac{\sqrt{\alpha_i^2 - 4\Gamma_i\beta_i}}{2\Gamma_i} \right]_{r_c} \quad (89)$$

where $[i = 1, 2, 3]$ corresponds to the constant height flow, conical flow and flow in vertical equilibrium, respectively. The set of quantities $[\alpha, \beta, \Gamma]_{i=1,2,3}$ can explicitly be obtained as

$$\begin{aligned}
 \alpha_1 &= \frac{2c(\gamma - 1 - c^2)(r_c - 1)}{(1 - c^2)r_c(r_c - 2)}, \\
 \beta_1 &= \frac{\beta'}{(-2 + r_c)^2 r_c^2 (r_c^3 - (-2 + r_c)\lambda^2)^2}, \\
 \Gamma_1 &= \frac{\gamma - 3u_c^2 + 1}{(1 - u_c^2)^2}
 \end{aligned} \quad (90)$$

where $\beta' = [\gamma\lambda^4 c_c^2 r_c^4 - 6\gamma\lambda^4 c_c^2 r_c^3 + 13\gamma\lambda^4 c_c^2 r_c^2 - 12\gamma\lambda^4 c_c^2 r_c + 4\gamma\lambda^4 c_c^2 - 2\gamma\lambda^2 c_c^2 r_c^6 + 8\gamma\lambda^2 c_c^2 r_c^5 - 10\gamma\lambda^2 c_c^2 r_c^4 + 4\gamma\lambda^2 c_c^2 r_c^3 + \gamma c_c^2 r_c^8 - 2\gamma c_c^2 r_c^7 + \gamma c_c^2 r_c^6 - \lambda^4 r_c^4 - \lambda^4 c_c^4 r_c^4 + 8\lambda^4 r_c^3 + 6\lambda^4 c_c^4 r_c^3 - 24\lambda^4 r_c^2 - 13\lambda^4 c_c^4 r_c^2 + \lambda^4 c_c^2 r_c^2 + 32\lambda^4 r_c + 12\lambda^4 c_c^4 r_c - 4\lambda^4 c_c^2 r_c - 4\lambda^4 c_c^4 + 4\lambda^4 c_c^2 + 2\lambda^2 c_c^4 r_c^6 + 3\lambda^2 r_c^6 - 8\lambda^2 c_c^4 r_c^5 - 20\lambda^2 r_c^5 + 10\lambda^2 c_c^4 r_c^4 + 48\lambda^2 r_c^4 - 2\lambda^2 c_c^2 r_c^4 - 4\lambda^2 c_c^4 r_c^3 - 40\lambda^2 r_c^3 +$

42 Tarafdar & Das

$$\begin{aligned}
& 4\lambda^2 c_c^2 r_c^3 - c_c^4 r_c^8 + 2c_c^4 r_c^7 - 2r_c^7 - c_c^4 r_c^6 + c_c^2 r_c^6 + 2r_c^6 - 16\lambda^4]_{r_c} \\
& \alpha_2 = \frac{2c(\gamma - 1 - c^2)(2r_c - 3)}{(1 - c^2)r_c(r_c - 2)}, \\
& \beta_2 = \frac{\beta''}{(-2 + r)^2 r^2 (r^3 - (-2 + r)\lambda^2)^2}, \\
& \Gamma_2 = \frac{\gamma - 3u_c^2 + 1}{(1 - u_c^2)^2}
\end{aligned} \tag{91}$$

where $\beta'' = [-36c^4\lambda^4 - 4c^4\lambda^4 r_c^4 + 28c^4\lambda^4 r_c^3 - 73c^4\lambda^4 r_c^2 + 84c^4\lambda^4 r_c + 8c^4\lambda^2 r_c^6 - 40c^4\lambda^2 r_c^5 + 66c^4\lambda^2 r_c^4 - 36c^4\lambda^2 r_c^3 - 4c^4 r_c^8 + 12c^4 r_c^7 - 9c^4 r_c^6 + 36c^2\gamma\lambda^4 - 12c^2\lambda^4 + 4c^2\gamma\lambda^4 r_c^4 - 28c^2\gamma\lambda^4 r_c^3 + 73c^2\gamma\lambda^4 r_c^2 - 84c^2\gamma\lambda^4 r_c - 8c^2\gamma\lambda^2 r_c^6 + 40c^2\gamma\lambda^2 r_c^5 - 66c^2\gamma\lambda^2 r_c^4 + 36c^2\gamma\lambda^2 r_c^3 + 4c^2\gamma r_c^8 - 12c^2\gamma r_c^7 + 9c^2\gamma r_c^6 - 2c^2\lambda^4 r_c^4 + 14c^2\lambda^4 r_c^3 - 35c^2\lambda^4 r_c^2 + 36c^2\lambda^4 r_c + 4c^2\lambda^2 r_c^6 - 20c^2\lambda^2 r_c^5 + 30c^2\lambda^2 r_c^4 - 12c^2\lambda^2 r_c^3 - 2c^2 r_c^8 + 6c^2 r_c^7 - 3c^2 r_c^6 - \lambda^4 r_c^4 + 8\lambda^4 r_c^3 - 24\lambda^4 r_c^2 + 32\lambda^4 r_c + 3\lambda^2 r_c^6 - 20\lambda^2 r_c^5 + 48\lambda^2 r_c^4 - 40\lambda^2 r_c^3 - 2r_c^7 + 2r_c^6 - 16\lambda^4]_{r_c}$

$$\begin{aligned}
& \alpha_3 = \frac{8c_c^2(\gamma - 1 - c_c^2)(-2\lambda^2 r_c + 3r_c^3 + 3\lambda^2)}{(\gamma + 1)^2 r_c u_c (-\lambda^2 r_c + r_c^3 + 2\lambda^2)}, \\
& \beta_3 = -\left[\frac{\beta_3''}{(\gamma + 1)^2 (r_c - 2)^2 r_c^2 (-\lambda^2 r_c + r_c^3 + 2\lambda^2)^2} \right]_{r_c}, \Gamma_3 = -\frac{4c_c^4}{(\gamma + 1)^2 u_c^2} + \frac{2(3\gamma - 1)c_c^2}{(\gamma + 1)^2 u_c^2} + \frac{u_c^2 + 1}{(u_c^2 - 1)^2}
\end{aligned} \tag{92}$$

The critical gradient of sonic velocities can be obtained by putting the values of $\left[\left(\frac{du}{dr}\right)_{r_c}\right]_i$ at eq. (43, 53, 61) for $i = 1, 2, 3$, respectively. For the constant height flow as well as the conical flow, $\left[u, c_s, \frac{du}{dr}, \frac{dc_s}{dr}\right]_{r_c}$ thus obtained can directly be substituted in eq. (15) to obtain the value of the acoustic surface gravity. For flow in hydrostatic equilibrium (along the vertical direction), $\left[u, c_s, \frac{du}{dr}, \frac{dc_s}{dr}\right]_{r_h}$ has to be obtained by integrating the flow equations using the corresponding values of the $\left[u, c_s, \frac{du}{dr}, \frac{dc_s}{dr}\right]_{r_c}$, and then by substituting $\left[u, c_s, \frac{du}{dr}, \frac{dc_s}{dr}\right]_{r_h}$ in eq. (15).

10.2. Determination of the location of the sonic horizon(s) and the critical velocity gradients at such horizons – Isothermal accretion.

Here, the first integral of motion of the following form (see, e.g., eq. (33–34))

$$\xi = \frac{r^2(r - 2)}{(r^3 - (r - 2)\lambda^2)(1 - u^2)} \rho^{\frac{2k_B}{\mu m_H} T} \tag{93}$$

serves as the equivalent of the energy first integral of motion in adiabatic flow[§] in connection with the computation of location of the critical points. The critical point

[§]For isothermal accretion total energy is not conserved.

conditions for the constant height flow is found to be

$$\left[u^2 = c_s^2 = \frac{-r^3 + (r-2)^2 \lambda^2}{r^3 - r^4 + (r-2)(r-1)\lambda^2} \right]_{r_c} \quad (94)$$

Substituting the expressions for the critical velocity and the critical sound speed (as obtained in the above equation) in eq. (93), we obtain the following 4th degree polynomial equation in r_c

$$\left[2c_s^2 r^4 - 2(1 + c_s^2) r^3 - 2\lambda^2 (c_s^2 - 1) r^2 - 2\lambda^2 (4 - 3c_s^2) r - 4\lambda^2 (c_s^2 - 2) \right]_{r_c} = 0 \quad (95)$$

The critical point condition and the corresponding polynomial equation for the conical flow can be obtained as

$$\left[u^2 = c_s^2 = \frac{-r^3 + (r-2)^2 \lambda^2}{3r^3 - 2r^4 + 6\lambda^2 - 7r\lambda^2 + 2r^2 \lambda^2} \right]_{r_c} \quad (96)$$

$$\left[4c_s^2 r^4 - 2(3c_s^2 + 1) r^3 - 2\lambda^2 (2c_s^2 - 1) r^2 + 2\lambda^2 (7c_s^2 - 4) r - 4\lambda^2 (3c_s^2 - 2) \right]_{r_c} = 0 \quad (97)$$

For both of the above flow configurations, r_c coincides with r_h as is obvious from the corresponding critical point conditions. For flow in vertical equilibrium, $r_c \neq r_h$ as is evident from the following critical point condition.

$$\left[u^2 = \frac{c_s^2}{1 + c_s^2} = \frac{-r^3 + (r-2)^2 \lambda^2}{8r^3 - 4r^4 + 10\lambda^2 - 11r\lambda^2 + 3r^2 \lambda^2} \right]_{r_c} \quad (98)$$

So for the following polynomial equation which is to be solved to obtain the critical points, a necessary but not sufficient condition of physically acceptable roots is $r_c > 2$, and r_h has to lie outside the event horizon.

$$\left[4r_c^4 c_s^2 - r^3 (1 + 8c_s^2) - r^2 \lambda^2 (-1 + 3c_s^2) - r \lambda^2 (4 - 11c_s^2) - 2\lambda^2 (-2 + 5c_s^2) \right]_{r_c} = 0 \quad (99)$$

The corresponding critical gradient of the advective velocity for three flow models can be expressed as

$$\left[\left(\frac{du}{dr} \right)_{r_c} \right]_{\text{CH}}^{\text{Isothermal}} = \left[\frac{\alpha_1^{\text{iso}}}{2\Gamma_1^{\text{iso}}} + \frac{\sqrt{\alpha_1^{\text{iso}2} + 4\beta_1^{\text{iso}} \Gamma_1^{\text{iso}}}}{2\Gamma_1^{\text{iso}}} \right]_{r_c} \quad (100)$$

$$\left[\left(\frac{du}{dr} \right)_{r_c} \right]_{\text{CF}}^{\text{Isothermal}} = \left[\frac{\alpha_2^{\text{iso}}}{2\Gamma_1^{\text{iso}}} + \frac{\sqrt{\alpha_2^{\text{iso}2} + 4\beta_2^{\text{iso}} \Gamma_1^{\text{iso}}}}{2\Gamma_1^{\text{iso}}} \right]_{r_c} \quad (101)$$

$$\left[\left(\frac{du}{dr} \right)_{r_c} \right]_{\text{VE}}^{\text{Isothermal}} = \left[\frac{\alpha_3^{\text{iso}}}{2\Gamma_3^{\text{iso}}} + \frac{\sqrt{\alpha_3^{\text{iso}2} + 4\beta_3^{\text{iso}} \Gamma_3^{\text{iso}}}}{2\Gamma_3^{\text{iso}}} \right]_{r_c} \quad (102)$$

The set of quantities $[\alpha^{iso}, \beta^{iso}, \Gamma^{iso}]_i$ can explicitly be obtained as

$$\begin{aligned}\alpha_1^{iso} &= -(3c_s^2 - 1) \left\{ (-1 + c_s^2 (r_c - 1)) r_c^3 - (2 + c_s^2 (r_c - 1) - r_c) (r_c - 2) \lambda^2 \right\} \\ \alpha_2^{iso} &= -(3c_s^2 - 1) \left\{ (-1 + c_s^2 (2r_c - 3)) r_c^3 - (2 + c_s^2 (2r_c - 3) - r_c) (r_c - 2) \lambda^2 \right\} \\ \alpha_3^{iso} &= - \left\{ (-1 + 4c_s^2 (r_c - 2)) r_c^3 - (2 + c_s^2 (3r_c - 5) - r_c) (r_c - 2) \lambda^2 \right\} \left(\frac{3c_s^2}{1 + c_s^2} - 1 \right) \\ \beta_1^{iso} &= c_s (1 - c_s^2) \left\{ (-3 + c_s^2 (4r_c - 3)) r_c^2 + (c_s^2 (3 - 2r_c) + 2 (r_c - 2)) \lambda^2 \right\} \\ \beta_2^{iso} &= c_s (1 - c_s^2) \left\{ (-3 + c_s^2 (8r_c - 9)) r_c^2 + (c_s^2 (7 - 4r_c) + 2 (r_c - 2)) \lambda^2 \right\} \\ \beta_3^{iso} &= \left\{ (-3 + 8c_s^2 (2r_c - 3)) r_c^2 + (c_s^2 (11 - 6r_c) + 2 (r_c - 2)) \lambda^2 \right\} \left\{ \frac{c_s}{(1 + c_s^2)^{\frac{3}{2}}} \right\} \\ \Gamma_1^{iso} &= 2r_c (r_c - 2) (r_c^3 - (r_c - 2) \lambda^2) c_s \\ \Gamma_3^{iso} &= 2r_c (r_c - 2) (r_c^3 - (r_c - 2) \lambda^2) c_s \sqrt{1 + c_s^2}\end{aligned}$$

Isothermal flow has position independent sound speed for obvious reason. Note that for *all* flow models for the isothermal accretion, the location of the critical points can be found completely analytically. For constant height flow as well as for the conical flow model, $[u, c_s, \frac{du}{dr}]_{r_c}$ thus obtained can directly be substituted in eq.(15), with a modification that $\frac{dc_s}{dr} = 0$, to obtain the value of the acoustic surface gravity. For flow in hydrostatic equilibrium (along the vertical direction), $[u, c_s, \frac{du}{dr}]_{r_h}$ has to be obtained by integrating the flow equations using the corresponding values of the $[u, c_s, \frac{du}{dr}]_{r_c}$, and then by substituting $[u, c_s, \frac{du}{dr}]_{r_h}$ in eq.(15), κ can be evaluated.

Acknowledgements

PT would like to acknowledge the kind hospitality provided by HRI, Allahabad, India, for several visits. The work of TKD has been partially supported by a research grant provided by S. N. Bose National Centre for Basic Sciences, Kolkata, India, under a guest scientist (long term sabbatical visiting professor) research programme. The authors acknowledge insightful discussions with Archan S Majumdar and would like to sincerely thank the anonymous referee for suggesting a number of useful improvements. Authors also acknowledge the help of Reema Chowdhury in correcting certain typos in the manuscript.

References

1. W. G. Unruh, 1981, Phys. Rev. Lett. 46, 1351
2. W. G. Unruh, 1995, Phys. Rev. D. 51, 2827
3. M. Visser, 1998, Class. Quant. Grav. 15, 1767
4. N. Bilić, 1999, Class. Quant. Grav. 16, 3953
5. Novello, Visser & Volovik (ed.) 2002, Artificial Black Holes. World Scientific, Singapore.
6. V. Cardoso, 2005, *Acoustic black holes*, physics/0503042

7. C. Barcelo, S. Liberati, and M. Visser, 2005, '*Analogue Gravity*', Living Reviews in Relativity, Vol. 8, no. 12, websource <http://relativity.livingreviews.org/Articles/lrr-2005-12/>, also at gr-qc/0505065
8. W. Unruh, R. & Schützhold, (ed), 2007, Quantum Analogues: From Phase Transitions to Black Holes and Cosmology, Springer, Lecture Note in Physics, Vol. 718
9. T. K. Das, 2004, Class. Quant. Grav. 21, 5253
10. S. Dasgupta, N. Bilić, and T. K. Das, 2005,
11. H. Abraham, N. Bilić, T. K. Das, 2006, Classical and Quantum Gravity, 23, 2371
12. T. K. Das, N. Bilic, & S. Dasgupta 2007, JCAP, 6
13. P. Mach, & E. Malec, 2008, Physical Review D, vol. 78, Issue 12, id. 124016 9
14. P. Mach, 2009, Reports on Mathematical Physics, vol. 64, issue 1-2, pp. 257-269
15. S. Nag, S. Acharya, A. K. Ray, T. K. Das, 2012, New Astronomy, Volume 17, Issue 3, p. 285-295
16. H-Y. Pu, I. Maity, T. K. Das, & H. K. Chang, 2012, Class. Quant. Grav. 29, 245020
17. N. Bilić, A. Choudhary, T. K. Das, & S. Nag, 2012, arXiv:1205.5506 [gr-qc]
18. A D Helfer, 2003, Rept. Prog.Phys., 66, 943
19. G. Rousseaux, C. Mathis, P. Mañssa, T. G. Philbin, & U. Leonhardt, 2008, New Journal of Physics, Volume 10, Issue 5, pp. 053015
20. G. Rousseaux, P. Mañssa, C. Mathis, P. Couillet, T. G. Philbin, & U. Leonhardt, 2010, New Journal of Physics, Volume 12, Issue 9, pp. 095018
21. G. Jannes, R. Piquet, P. Maissa, C. Mathis, & G. Rousseaux, 2011, Physical Review E, 83, 056312
22. S. Weinfurtner, E. W. Tedford, M. C. J. Penrice, W. G. Unruh, & G. A. Lawrence, 2011, Physical Review Letters, vol. 106, Issue 2, id. 021302
23. U. Leonhardt, & S. Robertson, 2012, New Journal of Physics, 14, 053003
24. S. J. Robertson, 2012, Journal of Physics B, Volume 45, Issue 16, pp. 163001
25. A.F. Illarionov, & R. A. Sunyaev 1975a, A & A, 39, 205
26. E. P. T. Liang, K. A. Thomson, 1980, ApJ, 240, 271
27. E. P. T. Liang, P. L. Nolan, 1984, Space Science Reviews, 38, 353
28. A. A. Bisikalo, V. M. Boyarchuk, V. M. Chechetkin, O. A. Kuznetsov, & D. Molteni 1998, MNRAS, 300, 39
29. A. F. Illarionov, 1988, Soviet Astron., 31, 618
30. L. C. Ho, 1999, in Observational Evidence For Black Holes in the Universe, ed. S. K. Chakrabarti (Dordrecht: Kluwer), 153
31. I. V. Igumenshchev & M. A. Abramowicz 1999, MNRAS, 303, 309
32. A. M. Beloborodov, & A. F. Illarionov 1991, MNRAS, 323, 167
33. I. V. Igumenshchev, & A. M. Beloborodov, 1997, MNRAS, 284, 767
34. D. Proga, & M. C. Begelman, 2003, ApJ, 582, 69
35. A. Janiuk, M. Sznajder, M. Mościbrodzka, & D. Proga, 2009, ApJ, 705, 1503
36. R. Matsumoto, S. Kato, J. Fukue, A. T. Okazaki, 1984, PASJ, 36, 71
37. J. Frank, A. King, D. Raine, 2002, Accretion Power in Astrophysics, Cambridge University Press, Cambridge
38. S. Kato, J. Fukue, & S. Mineshige, 1998, *Black Hole Accretion Disc*, Kyoto University Press.
39. R. H. Boyer, & R. W. Lindquist, 1967, J. Math. Phys. 8, 265
40. I. Novikov, & K. S. Thorne 1973, in Black Holes, eds. c. De Witt and B. De Witt (Gordon and Breach, New York).
41. Z. Meliani, C. Sauty, K. Tsinganos, & N. Vlahakis, 2004, A & A, Volume 425, pp. 773
42. D. Ryu, & I. Chattopadhyay, 2006, Astrophys. J. Suppl. Series, 166(1), 410
43. A. Migone, & J.C. McKinney, 2007, MNRAS, Volume 378, pp. 1118
44. S. Mondal, & P. Basu, 2011, Class. Quant. Grav., 28, 235004

45. B. Mukhopadhyay, & P. Dutta, 2012, *New Astronomy*, 17, 51
46. P. Tarafdar, & T. K. Das, 2013, arXiv:1305.7134 [gr-qc]
47. M. Anderson, 1989, *MNRAS*, 239, 19
48. T. K. Das, & B. Czerny, 2012b, *New Astronomy*, 17, 254
49. F. Yuan, S. Dong, & J-F. Lu, 1996, *Ap&SS* 246, 197
50. M. A. Abramowicz, & W. H. Zurek, 1981, *ApJ*, 246, 314
51. O. Blaes, 1987, *MNRAS*, 227, 975
52. B. Paczyński, P. J. Wiita, 1980, *A&A*, 88, 23
53. J. F. Lu, 1985, *A & A*, 148, 176
54. J. F. Lu, 1986, *Gen. Rel. Grav.* 18, 45L
55. J. F. Lu, K. N. Yu, & E. C. M. Young, 1995, *A & A*, 304, 662
56. C. F. Gammie, & R. Popham, 1998, *ApJ*, 498, 313
57. R. Popham, & C. F. Gammie, 1998, *ApJ*, 504, 419
58. J. F. Lu, K. N. Yu, F. Yuan, E. C. M. Young, 1997, *A & A*, 321, 665
59. J. F. Lu, K. N. Yu, F. Yuan, E. C. M. Young, 1997, *Astrophysical Letters and Communications*, 35, 389
60. J. F. Lu, & F. Yuan, 1998, *MNRAS*, 295, 66
61. J. F. Lu, & W. M. Gu, 2004, *Chin. Phys. Lett.*, 21, 2551
62. H. Riffert, & H. Herold, 1995, *ApJ*, 450, 508
63. J. P. Lasota, & M. A. Abramowicz, 1997, *Class. Quant. Grav.* 14, A237
64. M. A. Abramowicz, A. Lanza, & M. J. Percival, 1997, *ApJ*, 479, 179
65. L. D. Landau, & E. M. Lifshitz, 1994, *Statistical Mechanics*, Oxford: Pergamon, p. 125
66. S. Goswami, S. N. Khan, A. K. Ray, T. K. Das, 2007, *MNRAS*, 378, 1407
67. I. P. Bazarov, 1964, 'Thermodynamics', Pergamon Press, Oxford.
68. J. W. Gibbs, 1968, 'Elementary Principles in Statistical Mechanics', Dover, New York
69. D. W. Jordan, P. Smith, 1999, *Nonlinear Ordinary Differential Equations*, Oxford University Press, Oxford
70. C. Chicone, 2006, 'Ordinary Differential Equations with Applications', Springer; 2nd edition.
71. S. Strogatz, 2001, 'Nonlinear Dynamics And Chaos: With Applications To Physics, Biology, Chemistry, And Engineering', Westview Press; 1st edition.
72. W. J. M. Rankine, 1870, *Philosophical Transactions of the Royal Society of London* 160: 277
73. H. Hugoniot, 1887, *Journal de l'École Polytechnique* 57, 3
74. H. Hugoniot, 1887, *Journal de l'École Polytechnique* 58, 1
75. L. D. Landau, E. M. Lifshitz, 1987, 'Fluid Mechanics', Butterworth-Heinemann, Oxford
76. M. D. Salas, 'The curious events leading to the theory of shock waves', Invited lecture given at the 17th Shock Interaction Symposium, Rome, Italy, 4 - 8 September, 2006, 2006, *Shock Waves*, 16, 477
77. R. X. Yang, M. Kafatos, 1995, *A&A*, 295, 238
78. W. H. Press, S. A. Teukolsky, W. T. Vetterling, & B. P. Flannery, 2007, 'Numerical Recipes: The Art of Scientific Computing (3rd ed.)', New York: Cambridge University Press.
79. S. Liberati, S. Sonego, & M. Visser, 2000, *Classical and Quantum Gravity*, Volume 17, Issue 15, pp. 2903-2923
80. I. Hubeny, & V. Hubeny, 1998, *ApJ*, 505, 558
81. S. W. Davis, & I. Hubeny, 2006, *ApJS*, 164, 530
82. V. S. Beskin, 1997, *Phys. -Usp.* 40, 659
83. V. S. Beskin, & A. Tchekhovskoy, 2005, *A & A*, 433, 619
84. V. S. Beskin, 2009, *MHD Flows in Compact Astrophysical Objects: Accretion, Winds and Jets*. Springer.

85. A. G. Kurosh, 1972, Higher Algebra, Mir Publication, Moscow
86. G. F. l'Hôpital, 1696, Analyse des infiniment petits pour l'intelligence des lignes courbes, Paris.
87. S. Agarwal, T. K. Das, R. Dey, & S. Nag, 2012, General Relativity and Gravitation, 44, 1637
88. C. Barcelo, S. Liberati, S. Sonego & M. Visser, 2004, New J. Phys. 6 186 doi:10.1088/1367-2630/6/1/186
89. G. B. Rybicki, & A. P. Lightman, 1979, 'Radiative processes in astrophysics', New York, Wiley-Interscience
90. S. Kato, J. Fukue, & S. Mineshige, 1998, *Black Hole Accretion Disc*, Kyoto University Press.
91. S. Chandrasekhar, 1960, Proceedings of the National Academy of Sciences of the United States of America, Volume 46, Issue 2, pp. 253-257
92. S. A. Balbus, & J. F. Hawley, 1998, Reviews of Modern Physics, Volume 70, Issue 1, pp.1-53
93. N. I. Shakura, R. A. Sunyaev, 1973, A&A, 24, 337
94. D. B. Ananda, S. Bhattacharya, T. K. Das, 2014, 'Emergent acoustic causality and stability analysis for axisymmetric flows through perturbation of mass accretion rate', arXiv:1407.2268v3 [astro-ph.HE].
95. A. Recati, N. Pavloff, & I. Carusotto, 2009, Phys. Rev. A 80, 043603
96. S. Finazzi, & R. Parentani, 2011, Phys. Rev. D, 83, 084010
97. S. Finazzi, & R. Parentani, 2012, Phys. Rev. D, 85, 124027
98. A. Coutant, R. Parentani, S. Finazzi, 2012, 85, 024021
99. J. M. Miller, C. S. Reynolds, A. C. Fabian, G. Miniutti, & L. C. Gallo, 2009, ApJ, 697, 900
100. Y. Kato, M. Miyoshi, R. Takahashi, H. Negoro, & R. Matsumoto, 2010, MNRAS, 403, L74
101. J. Ziolkowski, 2010, Memorie della Societ  Astronomica Italiana, v.81, p.294
102. A. Tchekhovskoy, R. Narayan, & J. C. McKinney, 2010, ApJ, 711, 50
103. R. A. Daly, 2011, MNRAS, 414, 1253
104. S. D. Buliga, V. I. Globina, Y. N. Gnedin, T. M. Natsvlshvili, M. Y. Pitrovich, & N. A. Shakht, 2011, Astrophysics, Volume 54, Issue 4, pp.548
105. C. S. Reynolds, L. W. Brenneman, A. M. Lohfink, M. L. Trippe, J. M. Miller, R. C. Reis, M. A. Nowak, & A. C. Fabian, 2012, 'Probing Relativistic Astrophysics Around SMBHs: The Suzaku AGN Spin Survey', SUZAKU 2011: Exploring the X-ray Universe: Suzaku and Beyond. AIP Conference Proceedings, Volume 1427, pp. 157-164
106. J. E. McClintock, R. Narayan, S. W. Davis, L. Gou, A. Kulkarni, J. A. Orosz, R. F. Penna, R. A. Remillard, & J. F. Steiner, 2011, Classical and Quantum Gravity, Volume 28, Issue 11, pp. 114009
107. A. Martinez-Sansigre, & S. Rawlings, 2011, MNRAS, 414, 1937 114009
108. T. Dauser, J. Wilms, C. S. Reynolds, & L. W. Brenneman, 2010, MNRAS, 409, 1534
109. C. J. Nixon, P. J. Cossins, A. R. King, & J. E. Pringle, 2011, MNRAS 412, 1591
110. A. Tchekhovskoy, & J. C. McKinney, 2012, MNRAS, Online early. DOI: 10.1111/j.1745-3933.2012.01256.x
111. J. C. McKinney, A. Tchekhovskoy, & R. D. Blandford, 2013, Science, 339, 49
112. L. Brenneman, 2013, Measuring the Angular Momentum of Supermassive Black Holes, SpringerBriefs in Astronomy. ISBN 978-1-4614-7770-9
113. M. Dotti, M. Colpi, S. Pallini, A. Perego, & M. Volonteri, 2013, ApJ, 762, Issue 2, article id. 68, 10 pp.
114. A. Sesana, E. Barausse, M. Dotti, & E. M. Rossi, 2014, arXiv:1402.7088 [astro-ph.CO]
115. A. C. Fabian, M. L. Parker, D. R. Wilkins, J. M. Miller, E. Kara, C. S. Reynolds & T. Dauser, 2014, MNRAS, 439, 2307

- 116. J. Healy, C. Lousto, & Y. Zlochower, 2014, arXiv:1406.7295 [gr-qc]
- 117. J. Jiang, C. Bambi, & J. F. Steiner, 2014, arXiv:1406.5677 [gr-qc]
- 118. R. Nemmen, & A. Tchekhovskoy, 2014, arXiv:1406.7420 [astro-ph.HE]
- 119. D. Garfalo, 2013, 'Retrograde versus Prograde Models of Accreting Black Holes', *Advances in Astronomy*, vol. 2013, Article ID 213105, doi:10.1155/2013/213105, Online version <http://dx.doi.org/10.1155/2013/213105>